Electrochemical Deposition of SnS and FeS_xO_y Thin Films using Complexing Agents for Solar Cells Applications

Aizuddin bin Supee

Thesis submitted in partial fulfilment of the requirements for the award of the Doctoral (PhD) Degree of Engineering

Department of Engineering Physics, Electronics and Mechanics
Graduate School of Engineering
Nagoya Institute of Technology
Nagoya
Japan

March 2017

Electrochemical Deposition of SnS and FeS_xO_y Thin Films using Complexing Agents for Solar Cells Applications

和訳論文題目

太陽電池応用を目指した SnS、FeS_xO_y 薄膜の錯化剤を用いた電気化学堆積

Specially dedicated to my dearest father, mother, wife, son, family members and friends.

Acknowledgements

I wish to express my sincere appreciation to my supervisor, Prof. Dr. Masaya Ichimura for his willingness to accept me for joining his research group. His constant guidance, supports and advice comments throughout completion of this thesis are priceless and really helpful. I am also grateful to Dr. Masashi Kato for his useful comments and input during discussion.

My cordial gratitute to Prof. Tetsuo Soga and Assoc. Prof. Akio Wakejima for their time in reading and commenting my thesis. Their ideas and suggestions are valuable for my thesis improvement.

Thanks a lot to all Ichimura and Kato research group members for scientific discussion guide and technical assistance especially involving related laboratories facilities. Without them, definitely the learning process were difficult for the beginner like me.

A very special thanks goes to my father, Mr. Supee bin Omar, my mother, Mrs. Roimah binti Abdullah, my wife, Mrs. Nur'ain Balqis binti Haladin, and my son, Mr. Arif Zafran bin Aizuddin for their support and dedication.

Finally, I would like to thank all contributors in my research and thesis preparation for their encouragement and constructive advice.

Abstract

In this doctoral thesis, the electrochemical deposition (ECD) of semiconductor materials (SnS and FeS_xO_y thin films) either with or without complexing agents were studied. These materials are basically environmental friendly, non-toxic, and cheap, with abundance of the constituent elements in nature. Thus, they are viable as a candidate for low cost solar cells applications.

This thesis consists of seven chapters. In the first chapter, a brief background on solar cells, thin film deposition technologies, and the advantages of the selected ECD method are explained. In addition, the nature of available modes in ECD (potentiostatic, two and three steps pulse, galvanostatic), parameters governing ECD, and determination of deposition condition based on cyclic voltammetry (CV) are described. The basic material properties for solar cells applications (SnS, FeS_2, and ZnO) are also mentioned in this chapter.

In the second chapter, the effects of complexing agents on SnS thin films were studied. The SnS films were deposited on indium-tin-oxide (ITO)-coated glass substrate by three steps pulse ECD from a solution containing $Na_2S_2O_3$ and $SnSO_4$. Both ethylene-diaminetetraacetic (acid-EDTA[$CH_2N(CH_2COOH)_2]_2$) and L(+)-tartaric acid ($C_4H_6O_6$) with different concentration were added in the deposition solution. All the deposited SnS films exhibited p-type conductivity behaviour. The films with complexing agents generally showed less oxygen content and larger sulfur content than those deposited without the agents. The film thickness was decreased by addition of EDTA and low concentration of tartaric acid (< 10 mM), while it was slightly increased with a large amount of tartaric acid (> 30 mM). Larger crystalline size and larger optical transmittance were observed for SnS deposited with tartaric acid concentration larger than 30 mM.

In the third chapter, previous condition of SnS ECD with/without 100 mM tartaric acid was adopted in the fabrication of ZnO/SnS heterostructures. The 100 mM tartaric acid was selected based on larger optical transmittance, and no further reduction of oxygen content occurred for larger tartaric acid concentrations. Meanwhile, the heterostructure without tartaric acid was set for the comparison purposes. Initially, SnS

was deposited on ITO and then followed by the deposition of ZnO on SnS film by two steps pulse ECD from a solution of $Zn(NO_3)_2$. Both the heterostructures fabricated with/without tartaric acid showed clear rectifying properties. However, photovoltaic properties were not improved by the addition of tartaric acid.

In the fourth chapter, FeS_xO_y thin films were fabricated on the ITO substrate by galvanostatic ECD using a solution of $Na_2S_2O_3$ and $FeSO_4$. Both L(+)-tartaric acid and lactic acid ($CH_3CH(OH)COOH$) under different concentrations were used as the complexing agents. All the deposited films were amorphous. With the complexing agents, the thickness was increased, and oxygen content was reduced significantly compared with the sample deposited without the agents. In the photoelectrochemical measurement, p-type conductivity was confirmed. The photoresponsivity was not influenced significantly by the complexing agent, suggesting that the oxygen content does not drastically affect the properties of the deposited films probably because the local bonding configuration around Fe atoms in FeS_xO_y is not altered and similar to that in FeS_2.

In the fifth chapter, previous condition of FeS_xO_y ECD with/without complexing agents was implemented in the fabrication of ZnO/FeS_xO_y heterostructures. The 30 mM tartaric acid and 56 mM lactic acid were selected as the complexing agents in the FeS_xO_y depositions since there is no significant reduction in the oxygen content occurred exceeding these amount of concentrations. Meanwhile, the heterostructure without complexing agent was set for the comparison purposes. ZnO was deposited on FeS_xO_y by two steps pulse ECD from a solution containing $Zn(NO_3)_2$. For the ZnO/FeS_xO_y heterostructures fabricated with/without complexing agents, rectifying properties were confirmed in the current-voltage (J-V) characteristics. However, photovoltaic properties were not improved by the reduction of oxygen content in the FeS_xO_y film.

In the sixth chapter, three steps pulse electrochemical deposition was used to deposit FeS_xO_y thin films on indium-tin-oxide-coated glass substrates at room temperature from solution containing $Na_2S_2O_3$ and $FeSO_4$. The deposition was conducted under two different potential shifts direction (condition A: from negative to positive and condition B: from positive to negative) with intermediate potential V_2

variation. All the deposited films were amorphous. In Raman measurements, peaks attributed to marcasite and $Fe_{1+x}S$ were observed. The O/Fe ratio is larger than unity. The films under condition A with V_2 = -0.6 V and condition B with V_2 = -0.4 V showed a band gap which is estimated around 2.3-2.45 eV, larger than literature value of Fe_2O_3 (2.1 eV). In the photoelectrochemical measurement, n-type behaviour was confirmed.

Finally in the seventh chapter, the conclusion and recommendation for the future research are included.

Table of contents

List of tables

List of figures

Chapter 1

Introduction

1.1 Brief background on solar cells

The drive factors for the world's energy demand are strongly related to the population growth and the industrial evolution. It should be noted that the population has increased by 2 billion just in one generation and most of the contributor was from the developing countries [1]. Preventing energy crises is among the hottest issues being debated around the world nowadays. The energy demand is therefore significantly increased to satisfy the requirements of growing population and technology advancement for each country all over the world. As of the population growth and development initiatives, the conventional energy resources available in the world are depleting [2]. With higher conventional energy consumption, the pollution in the ecosystem increased tremendously due to the increment in the emission of various gases generated from the burning of fossil fuel. Since the conventional energy resources are not long-lasting and pollute the ecosystem, the dependency on these energy resources should be reduced. Thus, the developing countries are now putting their efforts in finding the alternative energy resources as replacement.

Currently, renewable energies such as wind energy, hydropower, geothermal and solar energy are extensively explored as the alternative energy resources. They offer advantages such as eco-friendly and theoretically non-exhausted source of energy, thus, capable to fulfill the world's energy demand. Among them, solar energy could be the best option since it is the most abundant energy resource. The sun emits the solar energy in various forms such as light and heat at the rate of 3.8×10^{23} kW and approximately 1.8×10^{14} kW is intercepted by the earth [3]. In addition, it can be used anywhere globally either in rural or town area, and requires relatively simple equipment design for energy conversion compared to other renewable energy. The solar energy extraction is basically accomplished through the use of solar cells. With these cells, the photon energy from the sunlight is converted into electricity.

Various types of solar cells have been introduced with impressive success for daily energy usage such as crystalline silicon (Si) and compound semiconductor thin films. At the moment, crystalline Si is mainly used in the market, and so far, the best reported efficiency obtained is greater than 20% [4-6]. The high cost of crystal substrate is the major drawback factor and reduction cost by ribbon crystal growth from the Si melt have been seriously considered. A well-developed photovoltaic panel able to withstand up to 10 years with 90% capacity and the capacity reduced to 80% for the following 15 years [7]. For the thin films such as $Cu(In,Ga)Se_2$ (CIGS) and CdTe, the best efficiencies were reported around 16% and 19% respectively [8]. Despite the efficiencies of both the thin films which are not far behind the crystalline Si, the high price of In and Ga coupled with the toxicity issue of Cd also limits the use of these compounds on a large scale.

Thin film technologies offer advantages such as flexible deposition process and good controllability of the surface and interface properties through the deposition parameters. However, the above limitations prompted intensive investigations on the alternative compounds that contain earth-abundant and low-cost elements. $Cu_2ZnSn(S,Se_4)$, SnS, Cu_2S, $CuSbS_2$, Cu_2O and FeS_2 are among the potential alternative materials for thin film solar cells. These materials consist of elements that are more abundant and lower in price as compared to CdTe and CIGS. However, the efficiencies of solar cells based on those mentioned alternative materials are still lower than CdTe and CIGS: 11.1% for $Cu_2ZnSn(S,Se)_4$ [9], 2.46% for SnS [10], 9.1% for Cu_2S [11], 3.1% for $CuSbS_2$ [12], 4.12% for Cu_2O [13], and 2.8% for FeS_2 [14]. Hence, it is important to fully develop these low cost materials so that the new-type of solar cells with high efficiency and good durability could be obtained.

Most of the thin films solar cells are operated based on p-n junction. Figure 1.1 illustrates the schematic of typical polycrystalline thin film solar cell. The junction (p-n) are formed by placing together the n-type (window layer-has an abundance of electrons) and p-type (absorber layer-has an abundance of holes) semiconductor materials. Near the junction of both layers, the electrons from the n-type layer diffuse to the p-type layer (where holes were initially present). Similarly, the holes flow by diffusion from the p-type layer to the n-type layer (where electrons were present). This movement creates an

area around the junction which is called as the depletion zone. The presence of these oppositely charged ions in the depletion zone creates an electric field that prevents electrons in the n-type layer to fill holes in the p-type layer. When the solar cell is irradiated by the photon (light) energy from the sun, the electrons are excited from the valence band to the conduction band, creating an extra mobile of electrons and holes (photo-generation of the charge carriers). The electric field makes the electrons flow to the n-type layer and the holes flow to the p-type layer. The resulting charges separation across the junction leads to the voltage formation. By connecting the solar cell to the external circuit, the electrons will travel from the n-type layer to the p-type layer by crossing the depletion zone and then go through the external circuit back of the n-type layer, creating a flow of electricity.

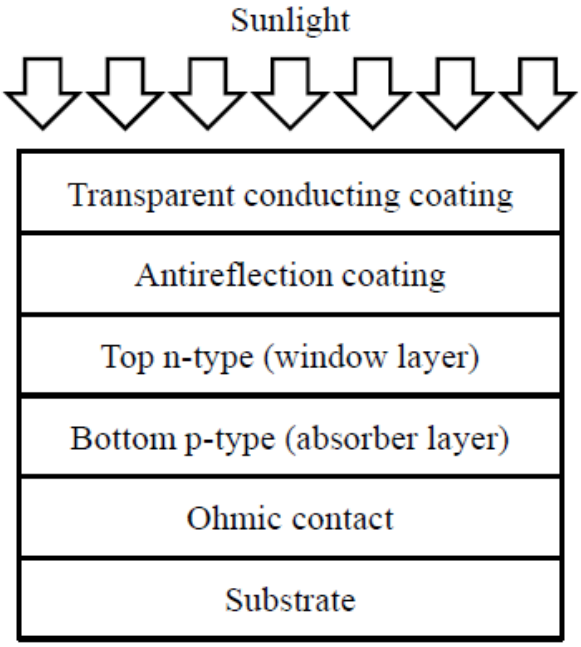

Fig. 1.1 Schematic of typical polycrystalline thin film solar cell.

1.2 Overview of thin film deposition technologies

Chopra et al. [15] defines a thin film as a material created ab initio by the random nucleation and growth processes of individually condensing/reacting atomic/ionic/molecular species on a substrate. The deposited thin film properties in terms of structural, physical, chemical and metallurgical were greatly influenced by the

deposition process, parameters and probably thickness. The thickness of the films may range from a few nanometers (nm) to tens of micrometers (μm). The thin films can be deposited either by physical or chemical methods. Thus, the factors such as the material suitability, advantages and limitation, and competitive cost should be taken into account during the selection of the deposition process.

1.2.1 Physical deposition methods

Physical methods cover the deposition process which depends on the evaporation or ejection of the material from a source, i.e. evaporation or sputtering. The physical methods are time-consuming process with a number of disadvantages such as sophisticated and costly instruments, need of skilled operators, compulsory vacuuming, wastage of material, cleaning of instrument after every deposition, size limitation of the substrates, and need of pure source materials. Basically, physical methods have been classified into evaporation and sputtering as discussed in the following:

- **Evaporation**

Evaporation or sublimation processes are widely used for the preparation of thin films. In evaporation, the substrate and source material are placed inside the vacuum chamber equipped with the heat source such as heater or laser. The source material in a container is then heated up to the evaporation temperature and at this point, the atoms/molecules start to leave the surface of the source material, heading towards the lower temperature surfaces such as the substrate or chamber wall. The atoms/molecules will transfer their energy to these surfaces, lower down their temperature and condense either on the substrate and/or on the chamber wall. The thickness of the deposited film is a function of the evaporation rate, the geometry of the source material and substrate, and evaporation time.

- **Sputtering**

The most basic and well-known mechanism involved in sputtering is the ejection of surface atoms from an electrode surface (source material) by momentum transfer from bombarding ions or energetic particles to surface atoms. Then, the ejected atoms will condense onto a substrate to form a thin film. Obviously, sputtering is an etching

process, and in fact, used for surface cleaning and for pattern delineation. Since sputtering produces a vapour of electrode material, this type of deposition is almost similar to evaporation deposition. However, this process has various advantages over evaporation: no container contamination will occur, and it is also capable to deposit alloy films which retain the composition of the source material.

1.2.2 Chemical deposition methods

Basically, the chemical methods are divided into vapour-phase and liquid-phase. Film formation by chemical processes in the vapour-phase includes chemical vapour deposition (CVD) and thermal oxidation. CVD involves flow of a precursor gas or gases (vapour) into a reaction chamber containing heated substrate. Chemical reactions occur near or on a substrate surface, resulting in the deposition of a thin film on the surface. This is accompanied by the production of chemical by-products that are exhausted out of the chamber together with unreacted precursor gases. The chemical reaction is an essential characteristic of this process, and therefore knowledge on chemical reactions involved must be well understood. Chemical reaction types basic to CVD include pyrolysis, reduction, oxidation, hydrolysis, synthetic chemical transport reaction, and etc. The deposition rate and the properties of the deposited films by CVD are significantly influenced by the deposition parameters such as temperature, pressure, input concentrations, gas flow rates, reactor geometry and operating principle. CVD processes possess the advantages such as production of films with high purity and uniform thickness, high density depending on the deposition conditions, and good control in composition.

On the other side, the growth of thin films in liquid-phase are accomplished primarily by electrochemical/chemical deposition process. Liquid-phase chemical reactions such as chemical bath deposition (CBD), successive ionic layer adsorption and reaction (SILAR), spin coating, and electrochemical deposition (ECD) offer a wide range of advantages over physical methods, being simple, economic and convenient for the deposition of thin films. The deposition parameters such as concentration, pH, nature of the complexing agent, temperature, and etc. are easily controllable and

manipulated. Since ECD was selected in this research, further discussion in the next section will be mainly focused and limited to the selected ECD process.

1.3 Electrochemical deposition (ECD) as the selected process for the deposition of thin films

Electrochemical deposition (ECD) is one of the most useful process and widely used to deposit thin films on the surface of conducting substrate. This process was successfully employed in the lab-scale to prepared numerous binary, ternary, and quaternary thin films semiconductors for solar cells applications such as SnS [16-18] and ZnO [19-20], Cu-Zn-S [21-22] and ZnCdO [23] and Cu_2ZnSnS_4 [24], and etc. In addition, this process is also implemented by Solo Power in their commercialized CIGS-based solar cell product. Figure 1.2 shows schematic of a standard three-electrode cell used for the deposition. Generally, the advantages of the ECD process can be listed as followed:

- The equipment setup is simple and low cost.
- The deposition process can be adopted at low temperature (room temperature) and atmospheric pressure condition.
- The properties of the films can be controlled accurately and easily by manipulating the deposition condition such as deposition current, voltage and time.
- It is capable of deposition on complex shapes and of large-scale production.

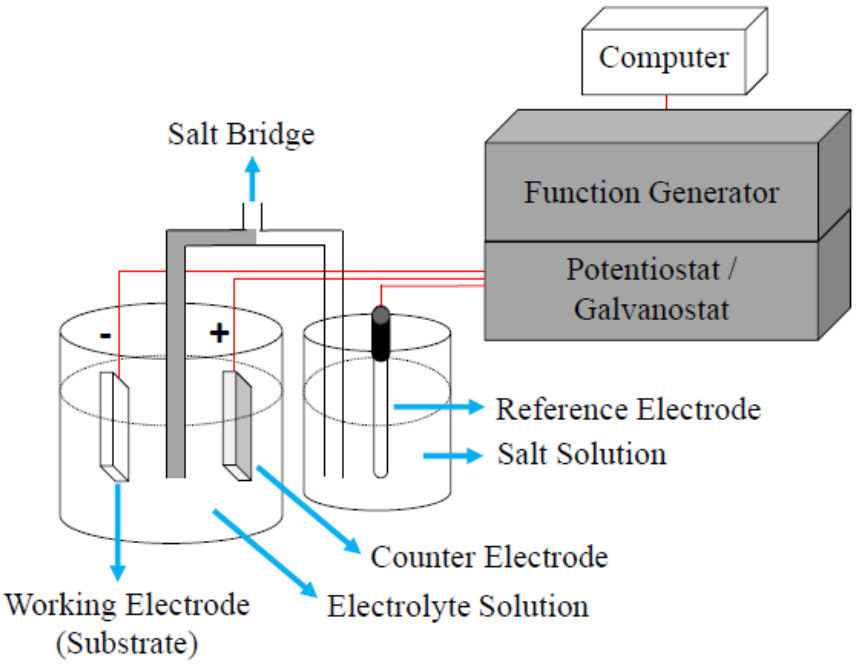

Fig. 1.2 Schematic of a standard three-electrode cell in ECD.

Despite the advantages being listed above, the ECD has its limits or drawbacks. The deposited films exhibit relatively poor quality and sometimes lack of long term stability. With the technologies advancement in the future, these disadvantages could be overcome. Moreover, the cost-effectiveness and the simplicity of the process would compensate or balance the weakness.

In ECD, the basic mechanism involved is the reaction between the ions which provided by an electrolyte solution and the surface of the working electrode (substrate). The deposition is controlled by an external applied potential/current. Thus, the electrical energy is used to cause chemical change. The ECD of ionic species from the electrolyte involves ionic transport from the bulk solution towards the substrate, and then discharge, followed by breaking of ion-ligand bond if the electrolyte solution is complex. The step was further continued with incorporation of the atoms on the substrate's surface, and followed by nucleation and growth either by surface diffusion or formation of clusters and critical nuclei, and lastly formation of monolayer and final growth of electrodeposits [25].

The properties of the deposited films in terms of structural, morphological and optical strongly depend on the ECD parameters such as substrate, electrolyte's concentration and temperature, pH of the solution, applied current densities/potentials, addition of complexing agents, and etc. These parameters should be properly controlled so that the uniform, smooth and stoichiometric films can be obtained [26-28]. The explanation of some of the parameters are as followed:

- Substrate

The selection of suitable types of substrate is essential in ECD because it can significantly affects the morphological characteristics of the growing layer as well as optical and electrical properties of the deposited films. The substrate should possess good conductivity to improve carrier collection efficiency, be mechanically stable in electrolyte solution, inert, have well-matched thermal expansion coefficient with the deposited layer to avoid cracking or peeling of the film, and also smooth surface to prevent local current distribution caused by uneven, porous, voids and other irregularities [15].

- Electrolyte solution's concentration

In ECD of thin films, the electrolyte solution acts as the source of an ionic species. By exerting current or potential to the ECD system, reaction occurred and this ionic species tends to be reduced on the substrate. Different concentration of chemicals used will cause different concentration of ionic species available in the electrolyte solution and hence affects the properties of the deposited films especially in term of composition.

- Electrolyte solution's temperature

The rising in temperature enhances the rate of diffusion and increases ionic species mobility and thus, increases the conductivity of the electrolyte solution. However, there exist the limits regarding to the suitability of the materials/films being used with increasing temperature. Proper ranges of temperature should be selected since it will affects the rate of nucleation and crystalline growth as well as morphology of the films [29-30].

- Hydrogen ion concentration (pH)

The presence of H^+ or OH^- ions in an aqueous electrolyte solution is unavoidable. High concentration of the OH^- ions (high pH value) may lead to the accumulation of hydroxide ions in the vicinity of the working electrode and form unnecessary precipitation, thereby altering the properties of the deposited film. The H^+ ions may cause the hydrogen gas evolution at the working electrode and thus, reduced the efficiency of the deposition [31]. Hence, the control of pH of electrolyte solution is vital so that the deposition process would be in optimum condition in order to maintain the desired film properties.

- Complexing agents

The use of complexing agents in the electrolyte solution is common in ECD of metals and they are expected to improve the electrolyte stability, produce sufficient adherence and smooth microstructure. The complexing agents will react with metal ions in the solution to form metal-complex, and these complex ions serve as reserves and continuously supply the required ions to be discharged at the working electrode. In other words, the release rate of the metallic ions can be slowed down or controlled so that stoichiometric film can be obtained in compound deposition [28,32]. Moreover, the complexing agents also prevent the formation of precipitation (e.g., metal hydroxide) or other undesired spontaneous reactions in the solution. Table 1.1 summarized examples of the previous work on the ECD of compound thin films with addition of complexing agent in the deposition solution.

Table 1.1 Previous works on ECD of thin films with addition of complexing agents in the deposition solution.

Reference no.	Type of thin films	Complexing agents	Effects on thin films
[33]	SnS	Lactic acid	Remove oxygen, better crystallinity, stoichiometric film.
[29]		Tartaric acid	Improve film uniformity and adherence, favoured S reduction.
[28,32]		EDTA	Retard Sn deposition rate, small grains, stoichiometric film.
[34]	ZnS	Sulfosalicylic acid	Suppress the formation of Zn and S impurity phases.
[35]	CIGS	Sulfamic acid	Promote the reduction of Ga^{3+}, inhibit the underpotential deposition of Cu-Se phases and the H^+ reduction into H_2.
[36]	FeS_xO_y	Tartaric acid, lactic acid	Increase film thickness, reduced oxygen content

1.3.1 Variant in ECD according to the nature of the selected modes

Since ECD was selected and used in fabrication of the thin films as discussed in the next chapter, it is best to describe the available modes in this process based on the selected external applied current or potential. Basically, the modes can be classified as followed:

- Direct current power supply at constant current (galvanostatic) mode

In the galvanostatic mode, the current flowing between the working electrode and the counter electrode is constant and can be controlled by a galvanostat. Meanwhile for the potential, it will takes on the value necessary to enable an electrochemical reaction to keep up with the current. The galvanostatic deposition is a complex process and requires knowledge on the current efficiency, current density and current

distribution as described by Faraday's law as well as maximum permissible growth rate for a good crystal formation.

The galvanostatic ECD of compound semiconductors is even more complex and there is no simple answer available in the selection of suitable current density for the deposition. Usually, the constituents in compound semiconductors are deposited by the means of migration, diffusion and convection. The migration involves the movement of ionic species under the action of an electric field to balance the charge flow in which the positive ions are attracted towards a negatively charged electrode meanwhile the negative ions are attracted towards a positively charge electrode. For the convection, the movement of species are driven by natural or forced mechanical force. The most simple and important one is diffusion in which the movement of ionic species are caused by the concentration gradient. The ions will flow from a region of high concentration to a region of low concentration.

For simplicity, the deposition of compound semiconductor is normally assumed under the category of diffusion controlled. In diffusion, the rate of deposition is directly proportional to the corresponding limiting current densities (the maximum current density that can be used to get a desired electrode reaction without undue interference). Thus, the galvanostatic ECD requires experiences and ability of the user to select an optimum ranges of current densities which is suitable for a specific compound semiconductor. In addition, initial trials or the series of experiments also could be useful to obtain the final optimum values of the electrodeposition current density.

- Direct current power supply at constant potential (potentiostatic) mode

In potentiostatic mode, the potentiostat will accurately control the potential of the working electrode against the reference electrode, and hence, the potential difference between the working electrode and the reference electrode is well defined and corresponds to the value specified by the user. This mode basically involves different charge transfer reactions occurring under a steady state condition at rates appropriate to the steady state interfacial overpotential and exchange current density. The overpotential selection is dictated by the composition of electrolyte solution, the substrate and the reversible potential of the ionic species to be deposited. Theoretically,

the potentials approximation at which electrodeposition of specific species would occur can be obtained via standard table of electrode potentials. However, in practical applications, the actual deposition is affected by the factors such as the substrate-deposit interaction, the hydrogen overvoltage, the interaction between the components during compound electrodeposition and the polarization characteristics of the electrolyte solution.

Potentiostatic deposition is carried out by the means of pure activation, diffusion or mixed control depending on the selection of the deposition potential. The potentiostatic deposition has been widely used to grow layers of elemental, binary and ternary semiconductors. For semiconductors, it is desirable to obtain large grained polycrystalline deposits. However, if very low overpotential is used, they may cause in spongy or porous deposit due to low nucleation rates. With increasing overpotential, the supersaturation will increase and large number of nuclei will be formed and thus the fine grained morphology for the deposit could be obtained. Meanwhile the very high overpotentials may lead to the growth of dendrites or whiskers. Therefore, more stringent control of the deposition potential is required for maintaining the stoichiometry and morphology of the electrodeposited compound semiconductors.

- Pulse power supply mode

Pulse is a process of deposition on the substrate using an interrupted direct current. In contrast to the direct current power supply at constant current (galvanostatic) and/or at constant potential (potentiostatic) modes, the sources (currents/potentials) are modified into the form of pulse and typical wave shapes used are involving sine and square. Examples of the square shape of pulse potentials are depicted in Fig. 1.3. Pulse electrochemical deposition allows manipulation of three independent parameters which are potentials/currents, on/off time for the potentials/currents, and number of cycles (total deposition time). These parameters are normally exploited to create a mass transport situation and promote electrocrystallization of the film through absorption and desorption effects and thus to determine the crystalline, compositional and optical properties of the deposited film.

During the "on" time, the more negative potential/current is applied meanwhile for the "off" time, the potential/current is less negative. The selected potentials/currents for the "on" and "off" time are basically obtained from the cyclic voltammetry (CV) which provide an information regarding to oxidation or reduction processes. The deposition (reduction) takes place at the "on" time where available ionic species in the layer close to the substrate are deposited. This results in decreased of ions concentration and thus at the "off" time, the concentration of ions will recover to compensate the ions consumed during the deposition. Moreover, weakly bonded part of the deposit may dissolve during “off” time, which causes an anodic peak. The "on" and "off" time in pulse deposition are vital. If the "on" time is too long, a lot of ions are consumed to be reduced at the substrate and if the "off" time is too short, shortage of ions supply occurs for the next "on" time. Therefore, it is essential to have a balance between "on" and "off" time so that the supply and demand for the ions will meet each other.

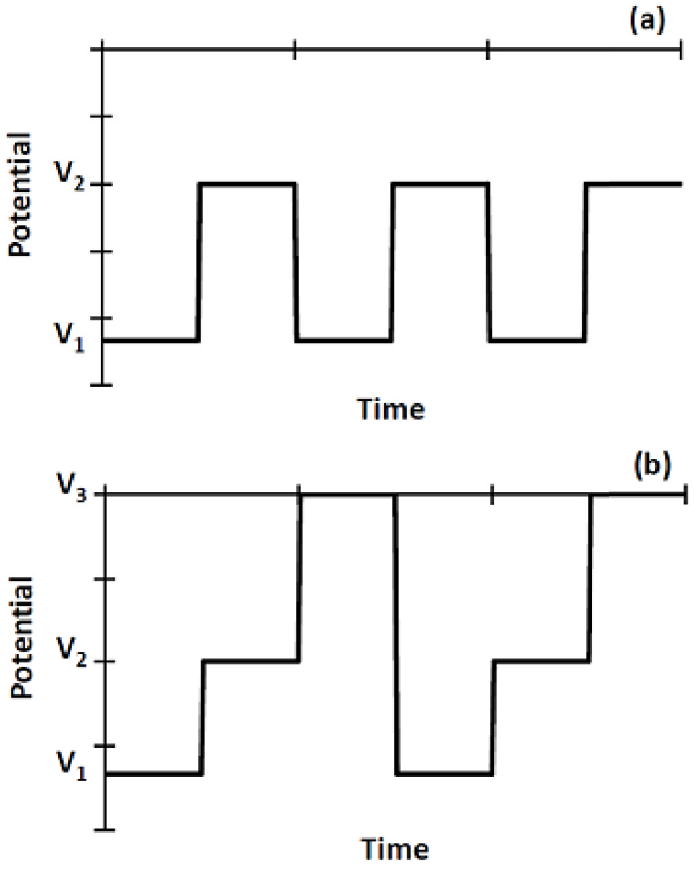

Fig. 1.3 Examples of the square shape of pulse potentials: (a) 2 steps pulse and (b) 3 steps pulse.

For the three steps pulse, similar deposition (reduction) and dissolution (oxidation) steps in the two steps pulse as mention previously were applied. In addition, the intermediate (diffusion) step then is introduced for equilibrating purposes. There is no effective reduction or oxidation current flowing during the diffusion step in a typical three step pulse deposition. The ions in the bulk electrolyte solution diffuse towards a layer near the substrate surface, which can affect the reaction rate of the next step (deposition or dissolution). Therefore, the overall deposition process can be modified by changing the intermediate step potential.

1.4 Cyclic voltammetry (CV)

Cyclic voltammetry (CV) technique is always the first option performed in order to get an insight of the preliminary information related to the deposition process. The CV is basically suitable for a study of all electrochemical reactions and could be applied without limitations. With CV aid, information about the type of reactions observed in the system and the potentials at which they occurred are easily obtained. The similar three-electrode cell setup like ECD (Fig. 1.2) is often used in CV. Standard CV experiments usually measure the current flowing through the working electrode (substrate) during a triangular potential perturbation. The applied potential is measured against the reference electrode, while the counter electrode closes the electrical circuit for the current to flow.

During the measurement, the potential is swept linearly from E_i (no electrode/substrate reactions occur) to E_1, then from E_1 to E_2 and lastly from E_2 to E_i [Fig. 1.4(a)]. The corresponding current is recorded as a function of the varying potential. An example of the plot is shown in Fig. 1.4(b) where the two anodic (A_{P1} and A_{P2}) and cathodic (C_{P1} and C_{P2}) peaks are observed and there is no visible current flows from E_i to E_s. It indicates that, the ionic species in the electrolyte solution can be deposited on the substrate when the values of negative (reduction) potential is between of E_s and E_1. Both anodic and cathodic peaks in CV normally represent activities of the ionic species which undergo complete oxidation and reduction process on the substrate surface. For complex ionic species, it is hard to determine at which potential/current each ionic species undergoes redox reactions. Usually, the peaks are overlapping and under the reduction process, the compound will be deposited on the substrate instead of

a single element. Thus, proper ranges of potential/current should be selected for the deposition, so that, the desired element/compound could be deposited.

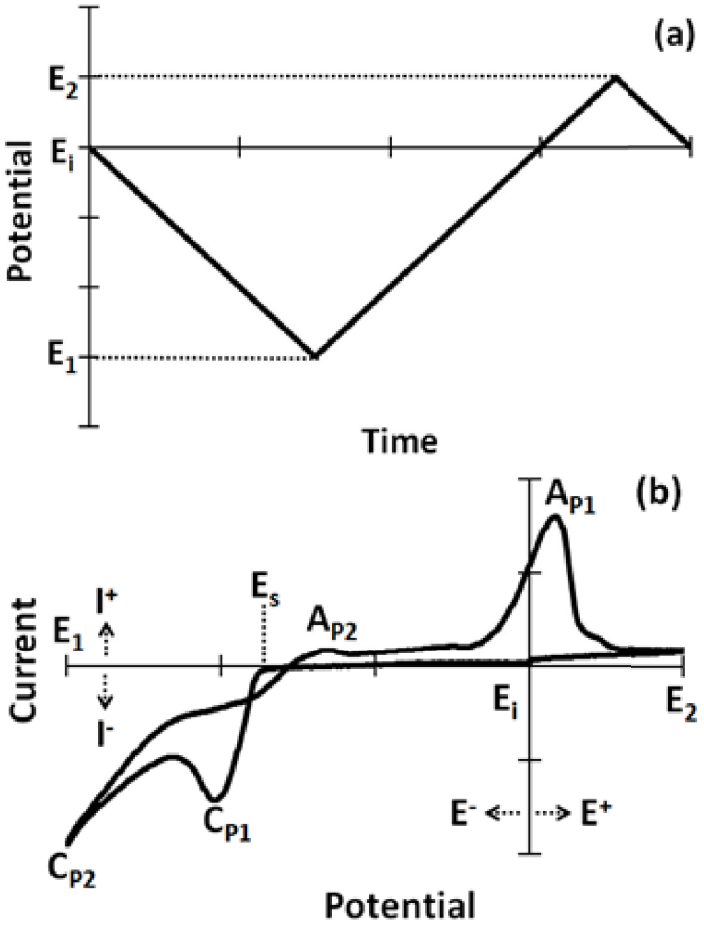

Fig. 1.4 Cyclic voltammetry: (a) triangular potential perturbation and (b) the corresponding current as a function of the varying potential.

1.5 Brief on basic material properties for solar cell applications

1.5.1 Tin sulfide (SnS)

An affordable solar energy for daily use is a common desired target in solar cells production. One of the possible way is by exchanging the higher cost of conventional Si material with another suitable materials. SnS from IV-VI group of semiconductor could be interesting since it contains non-toxic, cheaper and abundant elements in earth. Therefore, this material is well-matched for low cost solar cells. In addition, it also possesses favourable optoelectronic properties for solar cells application such as the

band gap energy around 1.1 eV similar to that of Si [37-38] and high absorption coefficient ($\alpha > 10^4$ cm^{-1}) in the visible wavelength ranges [39-40]. The direct and indirect band gap of SnS are estimated around 1.3-1.5 eV [39-42] and 1.0-1.1 eV [38,43-44] respectively, which is suitable for absorption of the solar radiation. Besides that, the SnS exhibits p-type photoresponse and thus served as an absorber layer in solar cells.

Hoffman [45] claimed that the SnS possesses an orthorhombic structure that may be described as pseudo-tetragonal in which every Sn atom is surrounded by three S atoms forming bond angles around 90˚. SnS has unit cell with lattice parameters of a = 4.336 Å, b = 11.143 Å, and c = 3.971 Å. Various processes have been reported in order to obtained SnS films such as chemical bath deposition [46], successive ionic layer adsorption and reaction [47], atomic layer deposition [48], vacuum evaporation [40,49], sulfurization of Sn metal [50], spray pyrolysis [42], electrochemical deposition [16,51], and others.

Electrochemical deposition under three steps pulse mode was selected to deposit SnS thin films and the properties of the electrodeposited SnS films either with or without complexing agents were discussed in chapter 2. Meanwhile, the effects of complexing agent in electrodeposited SnS films on ZnO/SnS heterostructures were elaborated in chapter 3.

1.5.2 Iron pyrite (FeS_2)

Iron pyrite (FeS_2) is a very attractive next-generation solar cell material since their elements are abundant in nature and non-toxic. The material extraction cost of FeS_2 was estimated to be $2x10^{-6}$ ¢/W and thus resulted in highest ranks in regards to the material availability among 23 existing semiconductor material systems that potentially lead to substantially lower costs than silicon [52]. Its cost effectiveness could be illustrated as a 4% efficiency of FeS_2 cell being equivalent to the 20% efficiency of single crystalline silicon solar [52-53]. In addition, FeS_2 has an advantage of high optical absorption coefficient ($\alpha > 10^5$ cm^{-1}) in the visible wavelength ranges [14,54]. Furthermore, it can exist in both n- and p-type [55] as well as both direct and indirect transition [54,56]. Therefore, owing to above mentioned properties, FeS_2 could be

adopted as an alternative material for absorber or window layer in solar cells applications.

To date, different methods have been reported to deposit FeS_2 thin films including sulfurization of iron films [57-58], magnetron sputtering [59-60], chemical bath deposition [61], spray pyrolysis [62-63], sol-gel deposition [64-65], electrochemical deposition [66-69], and others. In this research, an inexpensive and simple electrochemical deposition was selected to deposit FeS_2 thin films. The deposited films mainly contains significant amount of oxygen, thus the films were denoted as FeS_xO_y. The properties of the galvanostatic electrodeposited FeS_xO_y films with or without complexing agents were discussed in chapter 4. As a continuation to chapter 4, the effects of complexing agent in FeS_xO_y films on ZnO/FeS_xO_y heterostructures were presented in chapter 5. Meanwhile, the properties of the FeS_xO_y films deposited under three steps pulse were studied in chapter 6.

1.5.3 Zinc oxide (ZnO)

As one of the most significant oxide semiconductor material, ZnO from II-VI group has attracted considerable attention due to its excellent electrical, optical and piezoelectrical properties and its potential applications in various areas such as photocatalysis [70], optoelectronics, transducers, resonators [71], solar cells [72-73], gas sensors [74-75], and etc. ZnO is a semiconductor with a direct band gap around 3.2-3.4 eV [76-78] and normally forms in wurtzite crystal structure with a lattice parameters of a = 3.25 Å and c = 5.12 Å [76]. It has good photoconductivity (usually n-type) and a high optical transparency in the visible and infrared spectral regions, and therefore is suitable as a window layer in solar cells.

For heterostructures (ZnO/SnS and ZnO/FeS_xO_y) fabrication, two steps pulse electrochemical deposition was selected for ZnO. The implementation of ZnO as window layer in heterostructures was discussed in chapter 3 and chapter 5 respectively.

1.6 Objectives of the research

The final goal of this research is to develop cheaper and environmental friendly thin film solar cells with sufficient efficiencies for daily energy usage. Therefore, the

conventional materials which are expensive or toxic should be replaced with more viable ones, and/or the deposition process should be more cost-competitive. SnS and FeS_2 thin films deposited by ECD are among the best options available because both the material are non-toxic, cheap and abundant and because the deposition process is also simple and cost-effective for large scales production. Current status for both SnS and FeS_2 based solar cells is still far behind the theoretical prediction. For that reason, the initial action was taken to improve the properties of both the films (SnS and FeS_2) with hope that the improvements will also cause better efficiencies in solar cells. Thus, the objectives of the research are as follows:

- Deposit SnS thin films by three steps pulse ECD and investigate the effects of complexing agents (EDTA and tartaric acid) on the properties of the deposited films.

- Deposit FeS_xO_y thin films by galvanostatic ECD and investigate the effects of complexing agents (tartaric acid and lactic acid) on the properties of the deposited films.

- Fabricate the heterostructures with ZnO (ZnO/SnS and ZnO/FeS_xO_y) using selected complexing agents in the SnS and FeS_xO_y thin films and characterized the properties of the heterostructures.

- Deposit FeS_xO_y thin films by three steps pulse ECD and investigate the effects of potential shifts direction and intermediate voltage (V_2) towards the properties of the deposited films.

The scopes of the research only limited to the above mentioned. Other deposition parameters such as potentials/currents, deposition time and temperatures, and pH of the solution will not be considered, even though they significantly affect the properties of the deposited films. The types of complexing agents and the concentration used also limited to as described although there are a lot of other complexing agents which results in different effects on the film properties.

1.7 Organization of the thesis

The purpose of this research is to deposit thin films consisting of non-toxic, earth-abundant and low-cost elements i.e. SnS and FeS_xO_y for solar cell applications by using the simple and inexpensive ECD process. In this research, the effects of complexing agents on the properties of both deposited films were studied. In addition, different ECD modes were also used for the deposition. Then, the selected single films with/without complexing agents were applied in the heterostructures fabrication with ZnO as the n-type partner.

Overall, the thesis consists of seven chapters. In the first chapter, an overview of different thin film deposition methods was introduced. The advantages and disadvantages of ECD were explained, and relevant information on the deposition was described.

In the second chapter, SnS films were deposited on ITO-coated glass substrate by three steps pulse ECD from a solution of $Na_2S_2O_3$ and $SnSO_4$. Both EDTA and tartaric acid with different concentrations were used as the complexing agents.

In the third chapter, SnS ECD with/without 100 mM tartaric acid was implemented in the fabrication of ZnO/SnS heterostructures.

In the fourth chapter, galvanostatic ECD was applied in the deposition of FeS_xO_y films from a solution of $Na_2S_2O_3$ and $FeSO_4$. Both tartaric acid and lactic acid with different concentrations were used as the complexing agents.

In the fifth chapter, FeS_xO_y ECD without or with complexing agents (30 mM tartaric acid and 56 mM lactic acid) was used in the fabrication of ZnO/FeS_xO_y heterostructures.

In the sixth chapter, different potential shifts direction and intermediate potential V_2 were used in the three steps pulse ECD of FeS_xO_y films from a solution contained $Na_2S_2O_3$ and $FeSO_4$.

Lastly in the seventh chapter, the conclusion and recommendation for the future research were given.

References

[1] N. Kannan and D. Vakeesan, Renew. Sust. Energ. Rev. 62 (2016) 1092-1105.

[2] S. Shafiee and E. Topal, Energ. Policy 37 (2009) 181-189.

[3] N. L. Panwar, S. C. Kaushik, and S. Kothari, Renew. Sust. Energ. Rev. 15 (2011) 1513-1524.

[4] J. Zhao, A. Wang, M. A. Green, and F. Ferrazza, Appl. Phys. Lett. 73 (1998) 1991-1993.

[5] O. Schultz, S. W. Glunz, and G. P. Willeke, Prog. Photovolt: Res. Appl. 12 (2004) 553-558.

[6] K. Masuko, M. Shigematsu, T. Hashiguchi, D. Fujishima, M. Kai, N. Yoshimura, T. Yamaguchi, Y. Ichihashi, T. Mishima, N. Matsubara, T. Yamanishi, T. Takahama, M. Taguchi, E. Maruyama, and S. Okamoto, IEEE J. Photovolt. 4 (2014) 1433-1435.

[7] V. Devabhaktuni, M. Alam, S. Shekara Sreenadh Reddy Depuru, R. C. Green Ii, D. Nims, and C. Near, Renew. Sust. Energ. Rev. 19 (2013) 555-564.

[8] M. A. Green, K. Emery, Y. Hishikawa, W. Warta, and E. D. Dunlop, Prog. Photovolt: Res. Appl. 24 (2016) 3-11.

[9] T. K. Todorov, J. Tang, S. Bag, O. Gunawan, T. Gokmen, Y. Zhu, and D. B. Mitzi, Adv. Energy Mater. 3 (2013) 34-38.

[10] P. Sinsermsuksakul, K. Hartman, S. Bok Kim, J. Heo, L. Sun, H. Hejin Park, R. Chakraborty, T. Buonassisi, and R. G. Gordon, Appl. Phys. Lett. 102 (2013) 053901.

[11] J. A. Bragagnolo, A. M. Barnett, J. E. Phillips, R. B. Hall, A. Rothwarf, and J. D. Meakin, IEEE T. Electron Dev. 27 (1980) 645-651.

[12] W. Septina, S. Ikeda, Y. Iga, T. Harada, and M. Matsumura, Thin Solid Films 550 (2014) 700-704.

[13] Y. Nishi, T. Miyata, and T. Minami, Thin Solid Films 528 (2013) 72-76.

[14] A. Ennaoui, S. Fiechter, C. Pettenkofer, N. Alonso-Vante, K. Büker, M. Bronold, C. Höpfner, and H. Tributsch, Sol. Energy Mater. Sol. Cells 29 (1993) 289-370.

[15] K. Chopra, P. Paulson, and V. Dutta, Prog. Photovolt: Res. Appl. 12 (2004) 69-92.

[16] M. Ichimura, K. Takeuchi, Y. Ono, and E. Arai, Thin Solid Films 361–362 (2000) 98-101.

[17] Z. Zainal, M. Z. Hussein, and A. Ghazali, Sol. Energy Mater. Sol. Cells 40 (1996) 347-357.

[18] S. Cheng, Y. Chen, C. Huang, and G. Chen, Thin Solid Films 500 (2006) 96-100.

[19] S. Jiao, K. Zhang, S. Bai, H. Li, S. Gao, H. Li, J. Wang, Q. Yu, F. Guo, and L. Zhao, Electrochim. Acta 111 (2013) 64-70.

[20] N. Fathy and M. Ichimura, J. Cryst. Growth 294 (2006) 191-196.

[21] K. Yang, Y. Nakashima, and M. Ichimura, J. Electrochem. Soc. 159 (2012) H250-H254.

[22] M. F. de Carvalho, M. M. de Brito, and I. A. Carlos, J. Electroanal. Chem. 763 (2016) 81-89.

[23] M. Tortosa, M. Mollar, and B. Marí, J. Cryst. Growth 304 (2007) 97-102.

[24] G. Y. Kim, W. Jo, K. D. Lee, H.-S. Choi, J. Y. Kim, H.-Y. Shin, T. T. T. Nguyen, S. Yoon, B. S. Joo, M. Gu, and M. Han, Sol. Energy Mater. Sol. Cells 139 (2015) 10-18.

[25] R. K. Pandey, S. N. Sahu, and S. Chandra, Handbook of Semiconductor Electrodeposition, Marcel Dekker, Inc., New York, (1996) 304.

[26] D. Sarkar, X. Zhou, A. Tannous, M. Louie, and K. Leung, Solid State Commun. 125 (2003) 365-368.

[27] N. S. Gaikwad, V. M. Nikale, and C. H. Bhosale, J. Phys. Chem. Solids 64 (2003) 723-730.

[28] S. Cheng, Y. He, and G. Chen, Mater. Chem. Phys. 110 (2008) 449-453.

[29] J. R. Brownson, C. Georges, G. Larramona, A. Jacob, B. Delatouche, and C. Lévy-Clément, J. Electrochem. Soc. 155 (2008) D40-D46.

[30] S. Cheng, G. Chen, Y. Chen, and C. Huang, Opt. Mater. 29 (2006) 439-444.

[31] S. Sahu and C. Sanchez, J. Mater. Sci. Lett. 11 (1992) 1540-1542.

[32] S. Cheng, Y. He, G. Chen, E.-C. Cho, and G. Conibeer, Surf. Coat. Technol. 202 (2008) 6070-6074.

[33] F. Kang and M. Ichimura, Thin Solid Films 519 (2010) 725-728.

[34] X. Xu, F. Wang, J. Liu, Z. Li, J. Ji, and J. Chen, Thin Solid Films 520 (2012) 6864-6868.

[35] P. H. Quang, D. T. B. Hop, N. D. Sang, T. H. Duc, and L. T. Tu, J. Ceram. Process. Res. 13 (2012) S318-S322.

[36] A. Supee and M. Ichimura, Jpn. J. Appl. Phys. 55 (2016) 081202.

[37] M. Ristov, G. Sinadinovski, I. Grozdanov, and M. Mitreski, Thin Solid Films 173 (1989) 53-58.

[38] W. Albers, C. Haas, and F. van der Maesen, J. Phys. Chem. Solids 15 (1960) 306-310.

[39] M. Parenteau and C. Carlone, Phys. Rev. B 41 (1990) 5227-5234.

[40] H. Noguchi, A. Setiyadi, H. Tanamura, T. Nagatomo, and O. Omoto, Sol. Energy Mater. Sol. Cells 35 (1994) 325-331.

[41] P. Pramanik, P. K. Basu, and S. Biswas, Thin Solid Films 150 (1987) 269-276.

[42] N. Koteswara Reddy and K. T. Ramakrishna Reddy, Thin Solid Films 325 (1998) 4-6.

[43] K. Takeuchi, M. Ichimura, E. Arai, and Y. Yamazaki, Sol. Energy Mater. Sol. Cells 75 (2003) 427-432.

[44] S. C. Ray, M. K. Karanjai, and D. DasGupta, Thin Solid Films 350 (1999) 72-78.

[45] W. Hofmann, Z. Kristallogr. 92 (1935) 161-185.

[46] Y. Jayasree, U. Chalapathi, and V. Sundara Raja, Thin Solid Films 537 (2013) 149-155.

[47] B. Ghosh, S. Chowdhury, P. Banerjee, and S. Das, Thin Solid Films 519 (2011) 3368-3372.

[48] P. Sinsermsuksakul, J. Heo, W. Noh, A. S. Hock, and R. G. Gordon, Adv. Energy Mater. 1 (2011) 1116-1125.

[49] B. Ghosh, R. Bhattacharjee, P. Banerjee, and S. Das, Appl. Surf. Sci. 257 (2011) 3670-3676.

[50] K. T. Ramakrishna Reddy and P. Purandhara Reddy, Mater. Lett. 56 (2002) 108-111.

[51] K. Mishra, K. Rajeshwar, A. Weiss, M. Murley, R. D. Engelken, M. Slayton, and H. E. McCloud, J. Electrochem. Soc. 136 (1989) 1915-1923.

[52] C. Wadia, A. P. Alivisatos, and D. M. Kammen, Environ. Sci. Technol. 43 (2009) 2072-2077.

[53] C. Wadia, Y. Wu, S. Gul, S. K. Volkman, J. Guo, and A. P. Alivisatos, Chem. Mater. 21 (2009) 2568-2570.

[54] A. Ennaoui, S. Fiechter, W. Jaegermann, and H. Tributsch, J. Electrochem. Soc. 133 (1986) 97-106.

[55] A. L. Echarri and C. Sánchez, Solid State Commun. 15 (1974) 827-831.

[56] D. W. Bullett, J. Phys. C: Solid State Phys. 15 (1982) 6163-6174.

[57] L. Meng, J. P. Tu, and M. S. Liu, Mater. Lett. 38 (1999) 103-107.

[58] I. J. Ferrer and C. Sánchez, J. Appl. Phys. 70 (1991) 2641-2647.

[59] G. Willeke, R. Dasbach, B. Sailer, and E. Bucher, Thin Solid Films 213 (1992) 271-276.

[60] D. Lichtenberger, K. Ellmer, R. Schieck, and S. Fiechter, Appl. Surf. Sci. 70-71 (1993) 583-587.

[61] D. A. Mazón-Montijo, M. T. S. Nair, and P. K. Nair, ECS J. Solid State Sci. Technol. 2 (2013) P465-P470.

[62] A. Yamamoto, M. Nakamura, A. Seki, E. Li, A. Hashimoto, and S. Nakamura, Sol. Energy Mater. Sol. Cells 75 (2003) 451-456.

[63] R. H. Misho and W. A. Murad, Sol. Energy Mater. Sol. Cells 27 (1992) 335-345.

[64] L. Huang, F. Wang, Z. Luan, and L. Meng, Mater. Lett. 64 (2010) 2612-2615.

[65] H. Siyu, L. Xinyu, L. QingYu, and C. Jun, J. Alloys Compd. 472 (2009) L9-L12.

[66] K. Yang, S. Kawai, and M. Ichimura, Thin Solid Films 573 (2014) 1-5.

[67] S. Nakamura and A. Yamamoto, Sol. Energy Mater. Sol. Cells 65 (2001) 79-85.

[68] A. S. Aricò, V. Antonucci, P. L. Antonucci, E. Modica, S. Ferrara, and N. Giordano, Mater. Lett. 13 (1992) 12-17.

[69] A. Gomes, H. M. Mendonça, I. M. da Silva Pereira, and M. A. F. Costa, J. Solid State Electrochem. 4 (2000) 168-176.

[70] M. Boshta, M. O. Abou-Helal, D. Ghoneim, N. A. Mohsen, and R. A. Zaghlool, Surf. Coat. Tech. 205 (2010) 271-274.

[71] X. Y. Kong and Z. L. Wang, Nano Lett. 3 (2003) 1625-1631.

[72] J. Holmes, K. Johnson, B. Zhang, H. E. Katz, and J. S. Matthews, Appl. Organomet. Chem. 26 (2012) 267-272.

[73] A. Umar, Nanoscale Res. Lett. 4 (2009) 1004-1008.

[74] K. V. Gurav, V. J. Fulari, U. M. Patil, C. D. Lokhande, and O.-S. Joo, Appl. Surf. Sci. 256 (2010) 2680-2685.

[75] A. Ghosh, R. Sharma, A. Ghule, V. S. Taur, R. A. Joshi, D. J. Desale, Y. G. Gudage, K. M. Jadhav, and S.-H. Han, Sensors Actuat. B: Chem. 146 (2010) 69-74.

[76] D. P. Norton, Y. W. Heo, M. P. Ivill, K. Ip, S. J. Pearton, M. F. Chisholm, and T. Steiner, Mater. Today 7 (2004) 34-40.

[77] Ü. Özgür, Y. I. Alivov, C. Liu, A. Teke, M. A. Reshchikov, S. Doğan, V. Avrutin, S.-J. Cho, and H. Morkoç, J. Appl. Phys. 98 (2005) 041301.

[78] R. E. Marotti, P. Giorgi, G. Machado, and E. A. Dalchiele, Sol. Energy Mater. Sol. Cells 90 (2006) 2356-2361.

Chapter 2

Effects of complexing agents on three steps pulse electrodeposited SnS thin films

2.1 Introduction

In the SnS ECD method, the common type of solution used is tin (II) sulfate ($SnSO_4$) and sodium thiosulfate ($Na_2S_2O_3$) with addition of sulfuric acid (H_2SO_4) or hydrochloric acid (HCl) to adjust the pH. The quality of the deposited SnS film strongly relies on the electrolyte's composition used. The use of complexing agents is common in ECD of metals and is thought to improve electrolyte stability, produce sufficient adherence and smooth microstructure. For ECD of SnS also, it was reported that the complexing agents can make the composition more stoichiometric [1-2].

In this work, we carry out three steps pulse ECD of SnS thin films with two different complexing agents, i.e., ethylenediaminetetraacetic (acid-EDTA $[CH_2N(CH_2COOH)_2]_2$) and L(+)-tartaric acid ($C_4H_6O_6$). So far, effects of those complexing agents have been studied only for galvanostatic and DC potentiostatic ECD of SnS [1-3]. In addition, no comparison has been done for the effects of both EDTA and tartaric acid on SnS ECD. Hence, in this research, we discuss the effects of EDTA and tartaric acid on the three steps pulse ECD SnS film properties in terms of cyclic voltammetry (CV), thickness, surface morphology, composition ratio, crystalline structure, optical transmittance, and photoresponse. The SnS film without complexing agents is set as the control sample, and the effects of different concentrations of complexing agents are compared.

2.2 Experiments

A conventional three electrode cell was used in ECD with indium-tin-oxide (ITO)-coated glass substrate with resistivity of 10 Ω/cm^2 as the working electrode (WE), a platinum sheet as the counter electrode (CE) and a saturated calomel electrode (SCE) as the reference electrode (RE). The SCE was dipped into the beaker containing a

saturated KCl solution, and a glass tube filled with a saturated KCl solution was used for the salt bridge. Half of the solution in the tube was gelified using agar, to prevent intermixing with the deposition solution. The deposition area was fixed to 1 cm x 1 cm by masking and total deposition time was set to 7 min. Basic electrolyte solution contained 30 mM $SnSO_4$ and 100 mM $Na_2S_2O_3$ for the control sample, and different concentrations of the complexing agents ranging from 1 mM to 200 mM were added to the basic solution. However, for EDTA, it was limited to 10 mM due to the EDTA solubility limit in the solution. In the following, the complexing agent concentrations used were categorized as low and high. For "low", the concentrations were up to 10 mM, while for "high", the concentrations were greater than 10 mM. ECD was performed using periodic three steps pulse (potential: V_1 = -1 V vs SCE, on time t_1 = 10 s; V_2 = -0.6 V, t_2 = 10 s; V_3 = 0 V, t_3 = 10 s) at room temperature. Prior to each deposition, WE was cleaned using alkyl benzene and acetone, and rinsed with DI water. Meanwhile, CE was dipped into 30 ml sulfuric acid for 5 s, followed by ultrasonically rinsed with DI water. The pH of the electrolytes were not adjusted. Initial pH (before the deposition) of the electrolytes were as follows: SnS (control): 2.71, SnS with EDTA: 1 mM: 2.61, 3 mM: 2.58, 5 mM: 2.53, 10 mM: 2.21, SnS with tartaric acid: 1 mM: 2.54, 3 mM: 2.34, 5 mM: 2.31, 10 mM: 2.20, 30 mM: 1.83, 50 mM: 1.69, 100 mM: 1.56, 150 mM: 1.43, 200 mM: 1.39. After ECD process was completed, WE was cleaned with steady stream of DI water and then dried using N_2 gas.

The deposition and CV measurement were conducted using potentiostat/galvanostat HA-151B and function generator HB-305 (Hokuto Denko). In CV, the potential was swept from 0 V to -1.5 V followed by -1.5 V to 0.5 V and finally from 0.5 V to 0 V at 20 mV/s. Optical transmittance was measured in the range of 300 nm to 1500 nm wavelength using V-570 UV/VIS/NIR spectrophotometer (JASCO). Film thicknesses were measured by a profile meter Surfcom-1400D (Accretech-Tokyo Seimitsu). Surface morphology and compositional analysis were conducted using JAMP-9500F field emission Auger microprobe (JEOL) at a probe voltage of 10 keV and a current of $1x10^{-8}$ A. X-ray diffraction (XRD) patterns were recorded by SmartLab X-ray diffractometer (Rigaku) using a CuKα radiation source. Raman spectra were analyzed by laser Raman spectrophotometer-NRS-3300 (JASCO) using 632.8 nm red

laser as excitation source. Photoelectrochemical (PEC) measurements were carried out in an aqueous electrolyte containing 100 mM $Na_2S_2O_3$ under negative (0 V to -1 V) and positive (0 V to 1 V) potential scan. An Xenon lamp (80 mW/cm^2) was used as a source of light. The applied voltage was swept at 5 mV/s and the illumination was alternately switched on and off for each 5 s. All the characterization equipments mentioned above were operated at room temperature.

2.3 Results and discussion

Figure 2.1(a) illustrates CV for the SnS control sample, SnS with EDTA and low concentration (up to 10 mM) of tartaric acid. In Fig. 2.1(a), all the samples show clear anodic and cathodic peaks, and in the range of 0 V to about -0.60 V, there is no visible negative current appeared. Small shift of the cathodic peaks are observed, but the cathodic current density and curve shape are similar for all the samples.

The CV behaviours under high concentrations of tartaric acid (100 mM and 200 mM) were depicted in Fig. 2.1(b). Unlike Fig. 2.1(a), there is no visible cathodic current peaks observed, i.e., the cathodic current increased monotonically, and the anodic peaks shifted to a more negative potential compared to the control SnS solution. A curve shape similar to that of the control SnS was obtained by lowing pH to 1.54, with a minor anodic peak shift towards a more negative potential. However, the negative current is still lower than in the case of the high tartaric acid concentration. Thus, it can be conclude that the negative current was enhanced by addition of high tartaric acid concentration in the SnS deposition solution.

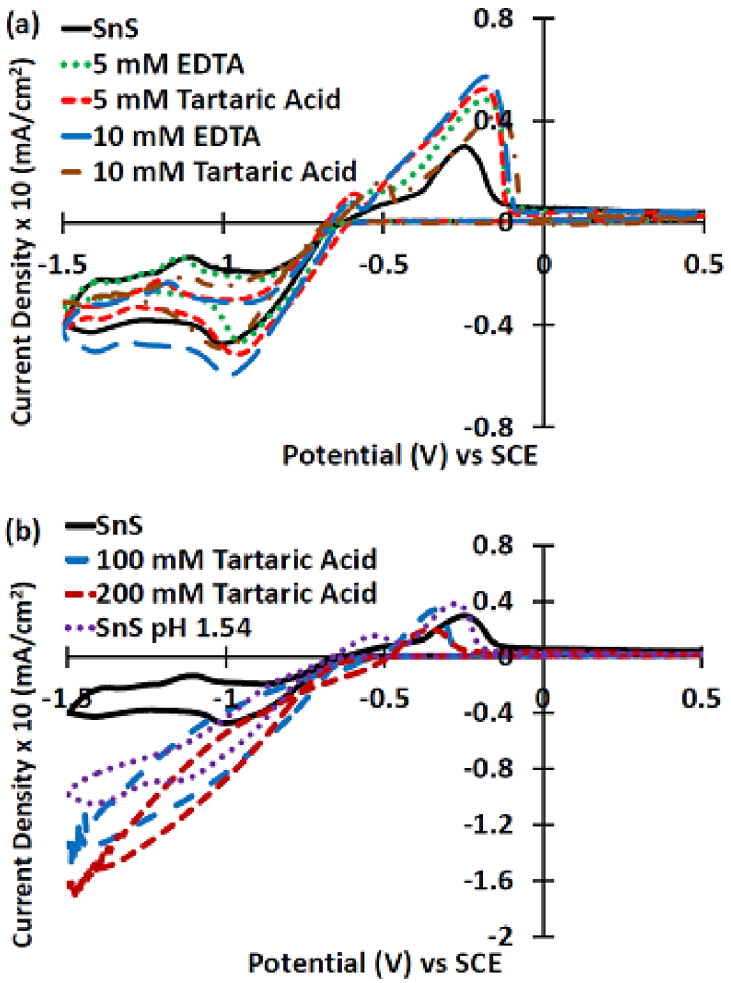

Fig. 2.1 Cyclic voltammetry for SnS samples: (a) SnS and low complexing agents concentration and (b) SnS and high concentration of tartaric acid.

Figure 2.2 shows the potential and current profile during the deposition. Compared with the control SnS deposition [Fig. 2.2(a)], there is no significant change in the profiles for the depositions with 10 mM EDTA [Fig. 2.2(b)], 10 mM tartaric acid [Fig. 2.2(c)] and 100 mM tartaric acid [Fig. 2.2(d)], although the positive current is smaller for the deposition with 10 mM EDTA. On the other hand, the positive current decreased significantly during the deposition when 100 mM tartaric acid was added.

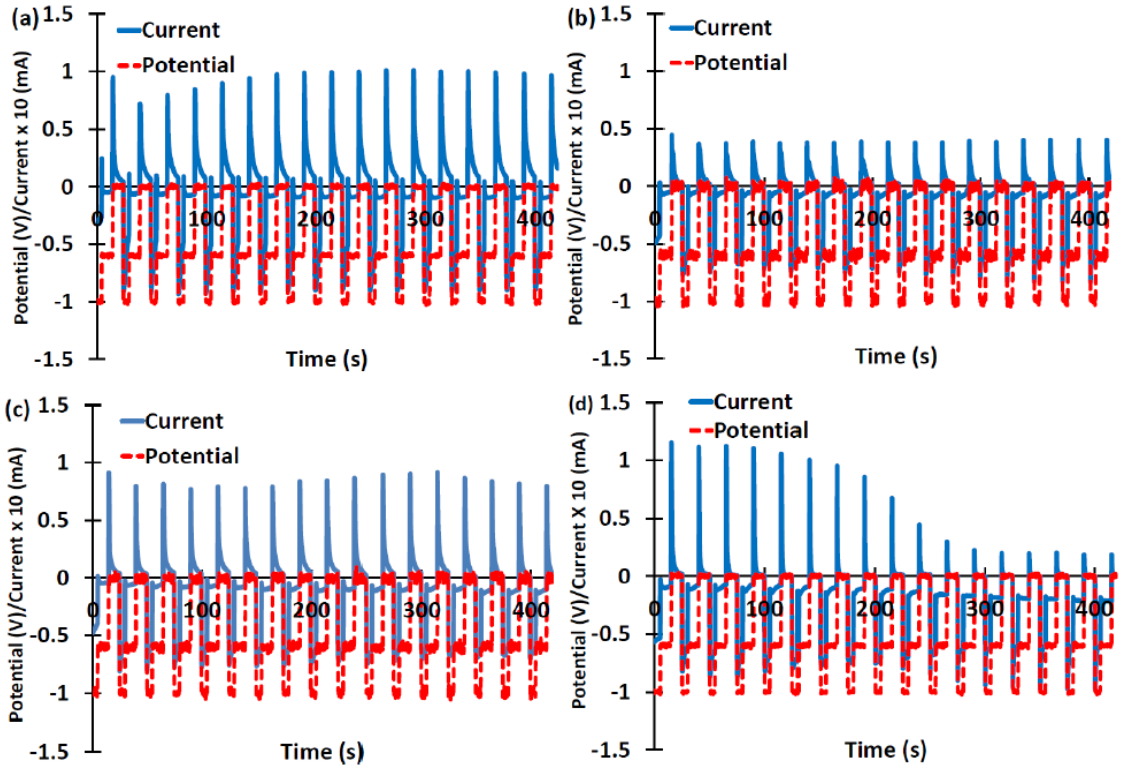

Fig. 2.2 Potential and current profiles during the deposition: (a) SnS, (b) 10 mM EDTA, (c) 10 mM tartaric acid, and (d) 100 mM tartaric acid.

Table 2.1 summarized the thickness measured for the deposited samples. Addition of low concentrations of both the complexing agents caused in thickness reduction compared to the SnS control sample. However, thicker SnS films were produced under high tartaric acid concentration (from 30 mM to 100 mM). Further increase in tartaric acid concentration exceeding 100 mM resulted in small film thickness reduction. The colour of the films also changed from dark brown (control SnS and SnS with low concentrations of EDTA or tartaric acid) to the dark grey (high tartaric acid concentration).

Table 2.1 Thickness of the deposited films.

Type of deposited film	Complexing agent concentration (mM)	Thickness (μm)	Direct band gap (eV)
SnS	0	0.25	-
SnS with EDTA	1	0.06	-
	3	0.04	-
	5	0.03	-
	10	0.03	1.45
SnS with tartaric acid	1	0.08	-
	3	0.05	-
	5	0.05	-
	10	0.05	1.32
	30	0.38	1.40
	50	0.50	1.57
	100	0.50	1.40
	150	0.30	1.35
	200	0.30	1.32

Figures 2.3(a)-2.3(f) show the selected scanning electron microscope (SEM) images for the deposited samples. The SnS control sample exhibited relatively large flower-like agglomerates of grains occurring on its surface. The increase in EDTA and tartaric acid concentration from 1 mM to 10 mM lead to reduced compactness of the grains, as can be seen in Figs. 2.3(c) and 2.3(e). Further increased in tartaric acid concentration up to 100 mM resulted in more dense agglomeration grains with more well defined boundaries. Although the films might seem to be not continuous and have some voids, the thickness profiles show that there is a continuous layer below the grains or the surface roughness. (The thickness values given in the table is the thickness of that continuous layer).

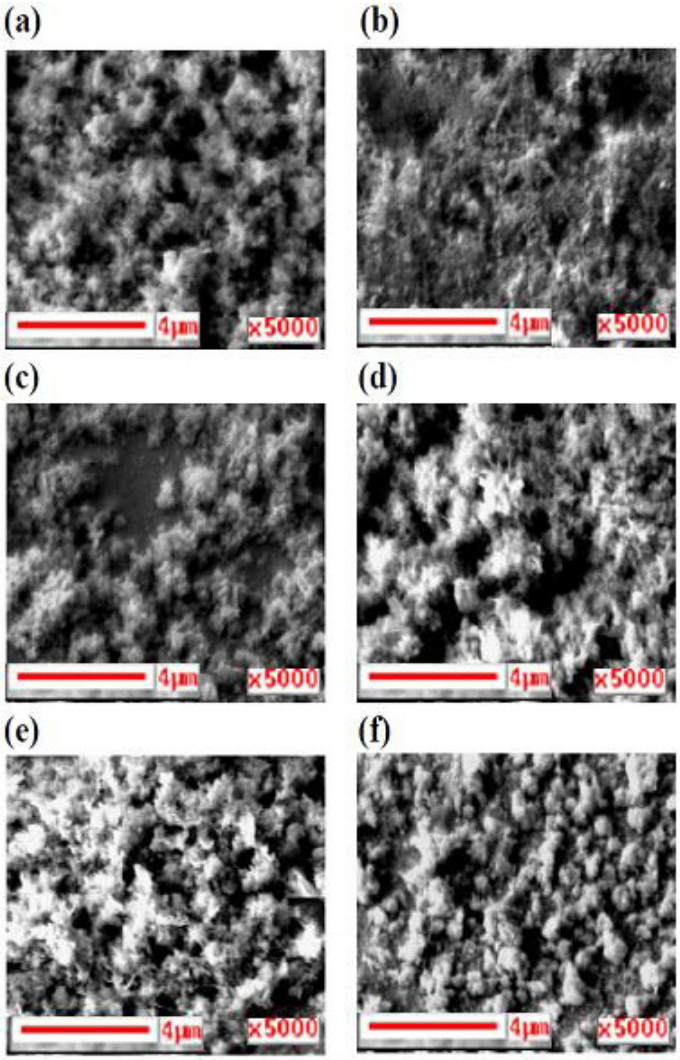

Fig. 2.3 SEM image of SnS deposited samples (Scale bar: 4 μm, x5000): (a) SnS, (b) 3 mM EDTA, (c) 10 mM EDTA, (d) 3 mM tartaric acid, (e) 10 mM tartaric acid, and (f) 100 mM tartaric acid.

Figure 2.4 illustrates Auger electron spectra (AES) for the SnS control sample. S/Sn and O/Sn ratios were calculated using a commercially available standard SnS and SnO_2 chemicals as the reference and are plotted in Figs. 2.5(a) and 2.5(b). In the ratio calculation, initially, the peak-to-peak intensity (from top to bottom) for each elements (S, Sn, O) were obtained from the AES spectra. Then, the peak intensities for S and O were divided with that of Sn (S/Sn, O/Sn). Finally, the calculated ratios (from the AES spectra) were divided with the respective reference ratios (S/Sn from SnS, O/Sn from SnO_2).

The oxygen content was reduced with increasing EDTA and tartaric acid concentration. The oxygen content further decreased when the tartaric acid concentration was greater than 10 mM as shown in Fig. 2.5(b). For the tartaric acid concentration greater than 50 mM, oxygen content was being constant and no further reduction occurred.

The sulfur content was also affected by the complexing agents concentration. Overall trends in Figs. 2.5(a) and 2.5(b) exhibit increasing sulfur content with increasing EDTA and tartaric acid concentration. These results show similarity with the previous works conducted [1-2,4].

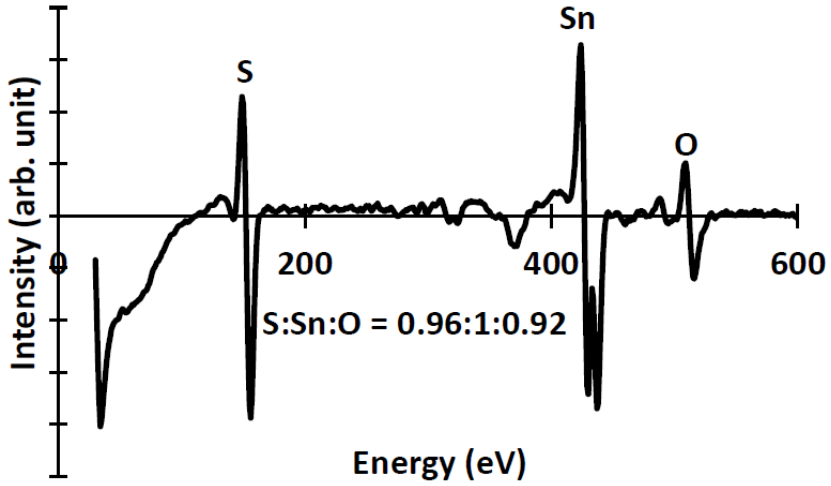

Fig. 2.4 AES for SnS control sample.

Figure 2.6 depicts XRD results for the selected deposited samples and ITO-coated glass substrate. The peaks for the deposited samples were compared with PDF card (00-039-0354), and the orthorhombic SnS peaks appear at $2\Theta = 31.97°$ for (040) and/or $2\Theta = 31.53°$ for (111). For the sample deposited with 100 mM tartaric acid, the SnS peak seems to be sharper than those of the others and be shifted to a lower angle: the peak is thought to be dominantly due to (111) diffraction rather than (040) diffraction. The small peak width indicates better crystallinity (larger crystalline grain size).

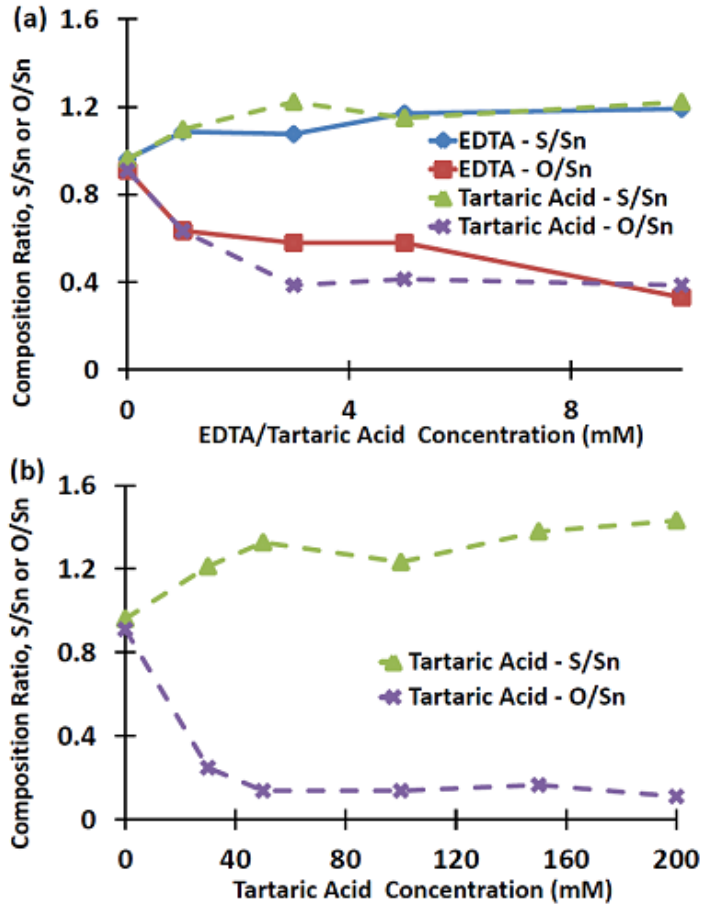

Fig. 2.5 (a) SnS and low concentration of complexing agents and (b) SnS and high concentration of tartaric acid - Compositional analysis by AES.

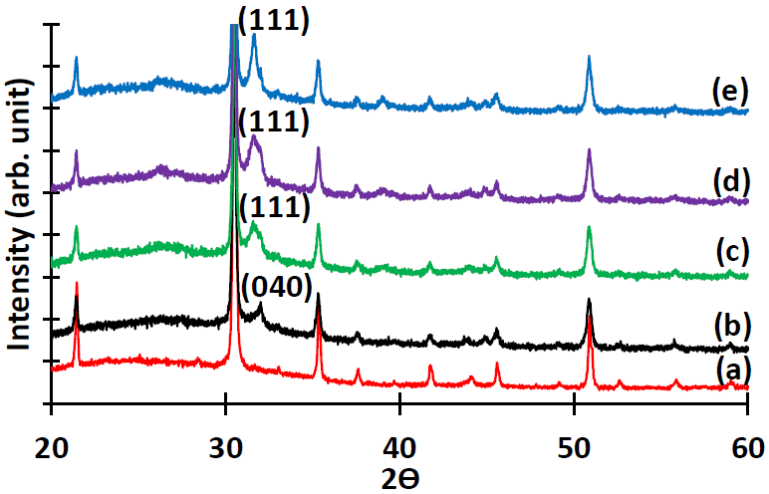

Fig. 2.6 XRD patterns for selected deposited samples: (a) ITO, (b) SnS, (c) 10 mM EDTA, (d) 10 mM tartaric acid, and (e) 100 mM tartaric acid.

Mathew et al. claim that the traces of SnS_2 and Sn_2S_3 in SnS films deposited by pulse electrodeposition can be observed through Raman spectroscopy [5]. To confirm the phase purity, Raman spectra were taken for the XRD measured samples. Raman peaks for crystalline SnS were observed at 70, 85, 95, 164, 192, 218 and 290 cm^{-1} [6], while for the measured samples, the peaks were detected at 100, 230, 293, 308, 314 cm^{-1} as shown in Fig. 2.7. The sample with 100 mM tartaric acid seems to be pure SnS without any other Sn-S phases (SnS_2 and Sn_2S_3) with a minor shift in Raman peak as compared to the previous work. Meanwhile, tiny phases of Sn_2S_3 and SnS_2 were observed in the samples with 10 mM tartaric acid and 10 mM EDTA respectively.

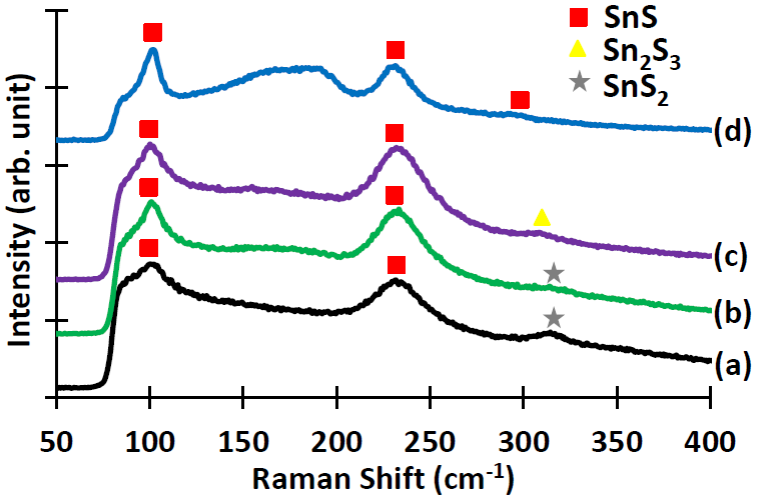

Fig. 2.7 Raman spectra for selected deposited samples: (a) SnS, (b) 10 mM EDTA, (c) 10 mM tartaric acid, and (d) 100 mM tartaric acid.

The optical transmittance were shown in Figs. 2.8(a)-2.8(d). The transmittance of the control SnS is low even in the IR range, and an absorption edge was not observed. The transmittance was increased by addition of the complexing agents. However, for the samples deposited with EDTA and with 1-10 mM tartaric acid, the film thickness is much smaller than the control SnS sample, and thus the enhanced transmittance will be mainly due to the reduced thickness. On the other hand, for the samples deposited with 30-200 mM tartaric acid, the thickness is comparable to or larger than that of the control sample, and still the transmittance is significantly higher.

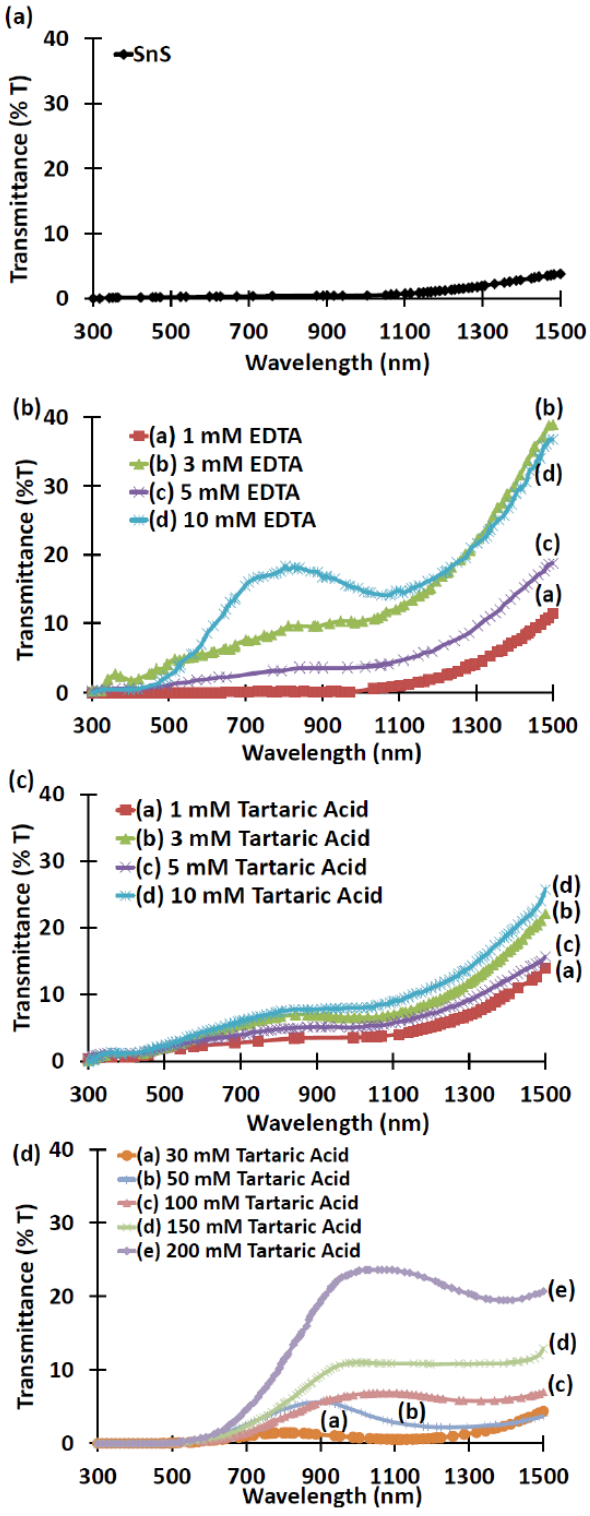

Fig. 2.8 Optical transmittance of the deposited samples: (a) SnS, (b) SnS with EDTA (low concentration), (c) SnS with tartaric acid (low concentration), and (d) SnS with tartaric acid (high concentration).

Clear optical transition slope was found in the samples deposited with 10 mM EDTA, and those with tartaric acid (greater than 3 mM), and thus the direct band gap was estimated for them by the plot of $(\alpha h\nu)^2$ vs. $h\nu$, where α is the absorption coefficient and $h\nu$ is the photon energy. The examples of the plot are shown in Fig. 2.9. The obtained band gap values are listed in Table 2.1. The band gap for the sample with 10 mM EDTA was evaluated to be 1.45 eV, which is in agreement with those of SnS films deposited with EDTA under DC potential [2]. On the other hand, for the SnS samples with tartaric acid, the band gap was in the range of 1.32 eV to 1.57 eV, different from those in the previous report of ECD with tartaric acid. Band gap energy estimated by the previous researcher for SnS with 200 mM tartaric acid was 1.05 eV and 1.09 eV when deposited at 70 ºC and 90 ºC, respectively [3].

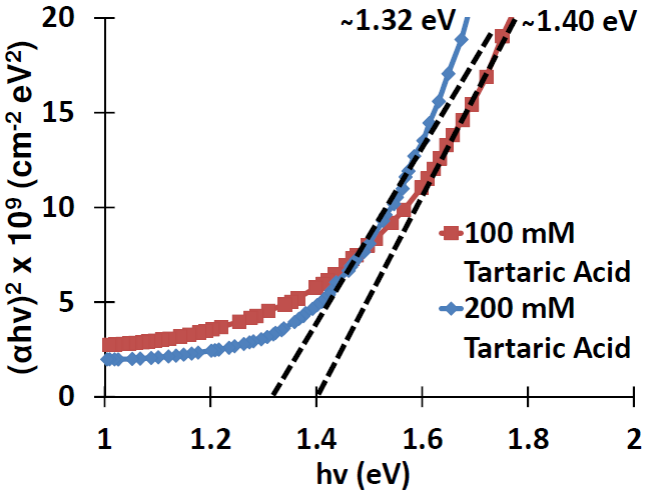

Fig. 2.9 $(\alpha h\nu)^2$ x 10^9 ($cm^{-2}eV^2$) versus $h\nu$ (eV) plot for the deposited samples.

Figure 2.10 depicts the photocurrent response in the PEC measurement for the sample with 1 mM EDTA under negative and positive potential scan. The negative potential scan exhibits larger photocurrent response compared to the positive potential scan. As the sample was illuminated, the current was increased, and then decreased as the illumination was interrupted. All the other tested samples (not shown here) exhibit similar photocurrent response as the sample with 1 mM EDTA. This indicates that the electron is the minority carrier in the samples, since the current due to the minority carrier is enhanced by the illumination more significantly than the majority carrier

current. Thus, it can be conclude that all the samples are photoactive and classified as p-type semiconductor. We confirmed that the SnS/ITO interface is not rectifying and thus does not have a significant energy barrier: an In/SnS/ITO structure exhibited ohmic current-voltage characteristics with low resistance. Thus, the observed photo response is due to the electrolyte/SnS interface.

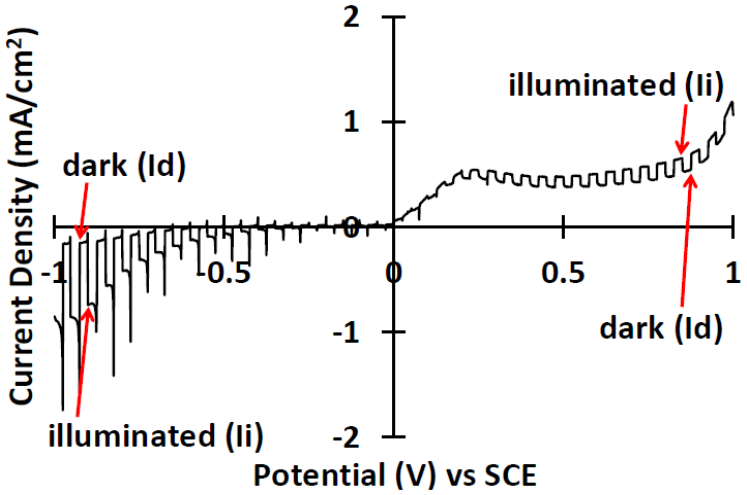

Fig. 2.10 Photocurrent response in PEC measurement of sample with 1 mM EDTA.

To gain better understanding of the photocurrent response for the tested samples, the difference between illuminated current (Ii) and dark current (Id) values at -0.80 V (negative potential scan) and 0.50 V (positive potential scan) were obtained. The difference was plotted against complexing agent concentration as shown in Figs. 2.11(a), 2.11(b) and 2.11(c). At -0.80 V, low concentration of both EDTA and tartaric acid (up to 10 mM) contributed to the larger photocurrent response compared to SnS control sample. This can partly be due to the decrease in the film thickness; since the sample is illuminated from the substrate side during the PEC measurement, a larger number of photons can reach the electrolyte/SnS interface with decreasing thickness. At higher tartaric acid concentration (30-200 mM), the negative response was smaller than for the control SnS as depicted in Fig. 2.11(b), which would be due to a larger film thickness.

At 0.50 V, the samples deposited with both the complexing agents resulted in smaller photocurrent response than the SnS control sample, as shown in Fig. 2.11(c). As noted above, the negative photoresponse of the samples deposited with the complexing

agents is larger than or comparable to that of the control sample. Since dominance of negative response is characteristic of p-type semiconductors, those results indicate that SnS tends to have clearer p-type character with addition of the complexing agents.

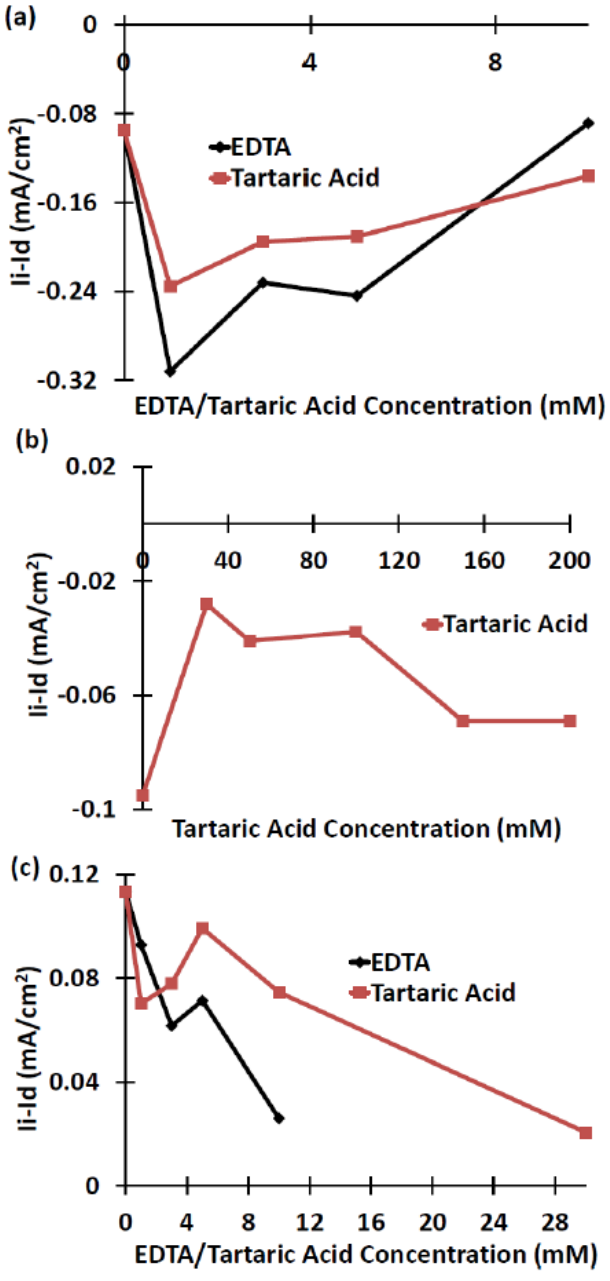

Fig. 2.11 (a) and (b) Comparison of the difference between the illuminated current and dark current (Ii-Id) of the tested samples at -0.8 V (negative potential scan), and (c) at 0.5 V (positive potential scan).

In ECD, the complexing agents are generally expected to form complex with metal ions and to prevent formation of precipitation (e.g., metal hydroxide) or other spontaneous reactions in the solution. In ECD of SnS, it was claimed in the previous works that the complex formation results in retardation of Sn deposition [1-2]. Then, the deposition of elemental Sn metal is suppressed, and the stoichiometric SnS can be obtained. In this work, with addition of EDTA or tartaric acid, the S/Sn ratio was increased as shown in Fig. 2.5. This will be due to the suppression of the Sn metal deposition by the complex formation. In addition, the O/Sn was decreased by the complexing agent, which could be due to the suppression of formation of $Sn(OH)_2$. Oxygen would be included in the film initially as $Sn(OH)_2$, which could then be decomposed into tin oxides. With a higher complexing agent concentration, free Sn^{2+} ion concentration was decreased, which results in suppression of $Sn(OH)_2$ formation and decrease in the oxygen concentration in the film.

However, in the case of EDTA and low concentration of tartaric acid, the deposition rate was significantly reduced. This is also thought to be due to the retardation of reduction of Sn ions. On the other hand, in the CV results, the negative current peak was not significantly influenced by EDTA or low concentration of tartaric acid. In the current profile shown in Fig. 2.2, the current profile was not influenced significantly by EDTA and low concentrations of tartaric acid, although the thickness was decreased. Apparently, with the low concentrations of the complexing agents in the solution, the negative current was consumed for reactions other than SnS deposition, such as H_2S generation.

When the tartaric acid concentration was increased to 30 mM or more, the CV and deposition results are quite different from the low concentration case. In the previous work, it was found that with 200 mM tartaric acid in the solution, the dominant current contributor is sulfur species [3]. Thus, it seems that tartaric acid can retard Sn reduction and accelerate S reduction. Owing to formation of the reduced S species (S^{2-}, S^{-}), SnS could be formed by the reaction

$$Sn^{2+} + S^{2-} = SnS \qquad (1)$$

A small amount of SnS_2 and Sn_2S_3 may also be formed so that S/Sn can exceed unity, as shown in Fig. 2.5. The samples deposited with the high concentrations of tartaric acid showed a sharper XRD peak and higher optical transmittance than the control sample. This will be due to the suppression of elemental Sn deposition. The reduction of the positive current in the current profile shown in Fig. 2.2 can also be due to decreased amount of elemental Sn, which can be dissolved during the positive pulse period more easily than the sulfides. Thus, we may conclude that tartaric acid can generally improve the properties of SnS films. However, the acceleration of the S reduction by tartaric acid can be significant only when the tartaric acid concentration is comparable to that of the sulfur source, i.e., thiosulfate ion (100 mM). Thus, at the low concentration (< 10 mM), only the retardation effect would be observed and the thickness was decreased.

The origin of the band gap variation is not clearly understood. There are numerous factors affecting the value of band gap, such as crystallinity (crystallite size) [7], impurities [4,8], native defect states [9-10], and phase purity [11-12]. The present results show that addition of the complexing agents influences oxygen content, phase purity, and crystallinity of the films. All of those factors may contribute to the band gap variation.

2.4 Conclusion

SnS thin films have been prepared on ITO-coated glass substrate at room temperature via three steps pulse ECD from an aqueous bath containing $SnSO_4$ and $Na_2S_2O_3$, and the effects of two complexing agents, EDTA and tartaric acid were studied. The films deposited with the complexing agents generally show less oxygen content and larger sulfur content than those deposited without the agents. The film thickness was decreased by addition of EDTA and low concentration of tartaric acid (< 10 mM), while it was slightly increased with a large amount of tartaric acid (> 30 mM). Crystallinity and optical transmittance were improved when tartaric acid concentration was larger than 30 mM. The effects of tartaric acid can be explained considering suppression of elemental Sn deposition and enhancement of sulfur reduction.

References

[1] S. Cheng, Y. He, and G. Chen, Mater. Chem. Phys. 110 (2008) 449-453.

[2] S. Cheng, Y. He, G. Chen, E.-C. Cho, and G. Conibeer, Surf. Coat. Technol. 202 (2008) 6070-6074.

[3] J. R. Brownson, C. Georges, G. Larramona, A. Jacob, B. Delatouche, and C. Lévy-Clément, J. Electrochem. Soc. 155 (2008) D40-D46.

[4] A. Ghazali, Z. Zainal, M. Zobir Hussein, and A. Kassim, Sol. Energy Mater. Sol. Cells 55 (1998) 237-249.

[5] N. R. Mathews, H. B. M. Anaya, M. A. Cortes-Jacome, C. Angeles-Chavez, and J. A. Toledo-Antonio, J. Electrochem. Soc. 157 (2010) H337-H341.

[6] H. R. Chandrasekhar, R. G. Humphreys, U. Zwick, and M. Cardona, Phys. Rev. B 15 (1977) 2177-2183.

[7] R. Ramírez-Bon, F. J. Espinoza-Beltrán, H. Arizpe-Chávez, O. Zelaya-Angel, and F. Sánchez-Sinencio, J. Appl. Phys. 77 (1995) 5461-5463.

[8] M. Innocenti, L. Becucci, I. Bencistà, E. Carretti, S. Cinotti, L. Dei, F. Di Benedetto, A. Lavacchi, F. Marinelli, E. Salvietti, F. Vizza, and M. L. Foresti, J. Electroanal. Chem. 710 (2013) 17-21.

[9] S. P. Patel, A. K. Chawla, R. Chandra, J. Prakash, P. K. Kulriya, J. C. Pivin, D. Kanjilal, and L. Kumar, Solid State Commun. 150 (2010) 1158-1161.

[10] K. Das, S. K. Panda, S. Gorai, P. Mishra, and S. Chaudhuri, Mater. Res. Bull. 43 (2008) 2742-2750.

[11] F. Smaïli, M. Kanzari, and B. Rezig, Mater. Sci. and Eng.: C 28 (2008) 954-958.

[12] M. Devika, N. K. Reddy, K. Ramesh, K. R. Gunasekhar, E. S. R. Gopal, and K. T. R. Reddy, J. Electrochem. Soc. 153 (2006) G727-G733.

Chapter 3

Effects of tartaric acid on electrochemical deposition of SnS in ZnO/SnS heterostructures

3.1 Introduction

The theoretical conversion efficiency of a SnS-based solar cell can reach 25% [1]. Different researcher used different processes in SnS deposition and selected different materials for the n-type window layer. Noguchi et al. [2] and Ghosh et al. [3] deposited SnS via vacuum evaporation and fabricated CdS/SnS heterostructures, which resulted in efficiency less than 0.3%. Ristov et al. [4] fabricated photovoltaic cells with different window layers such as CdO, Cd_2SnO_4 and SnO_2:F using chemical bath deposited SnS. Thermal evaporation of SnS was applied for SnS/ZnO heterostructures [5]. Heterostructures with ZnO-based alloys (Zn(SO), (ZnMg)O, (ZnSn)O) were also fabricated recently [6-8]. Pulse electrochemical deposition (ECD) of SnS was adopted by Ichimura et al. [9] and Gunasekaran et al. [10] for heterostructure fabrication with ZnO and CdS, respectively.

Several groups have successfully improved the properties of electrodeposited SnS films with addition of complexing agents in the deposition solution [11-14]. In our previous work [15], tartaric acid ($C_4H_6O_6$) was used as a complexing agent in three steps pulse ECD of SnS. Addition of 100 mM tartaric acid resulted in larger film thickness, larger optical transmittance, comparable p-type conductivity, better surface morphology and crystallinity, enhanced sulfur content, and reduced oxygen content in the film.

In the present study, we further implement our previous condition of SnS ECD with 100 mM tartaric acid in ZnO/SnS heterostructure fabrication. ZnO was selected as window layer material and it was deposited by two steps pulse ECD [9]. Both SnS and ZnO consist of abundant and nontoxic elements, and thus the ZnO/SnS heterostructure is well suited for low-cost solar cells. A heterostructure with SnS fabricated without tartaric acid was set as a control sample, and the effects of 100 mM tartaric acid on the

heterostructure properties were investigated. To our knowledge, fabrication of heterostructures based on ECD SnS deposited with a complexing agent is attempted for the first time in this study.

3.2 Experiments

The same approaches as described in chapter 2 were used in the SnS deposition and characterization of the films/heterostructures including thickness measurement, X-ray diffraction (XRD), surface morphology observation, and elemental compositional ratio calculation. The cross-sectional SEM images were observed via JSM 7001FF (JEOL) at a probe voltage of 15.0 kV and a current of 57.0 x 10^{-6} A.

SnS was initially deposited on ITO either without (control sample) or with 100 mM tartaric acid. Initial pH of the electrolytes and the thicknesses of the films were as follows: SnS control: 3.04 (0.4 μm), SnS with 100 mM tartaric acid: 1.90 (0.75 μm).

As a counterpart of SnS, ZnO was deposited on SnS using two steps pulse (potential: V_1 = -1.3 V vs SCE, on time t_1 = 10 s; V_2 = -0.6 V, t_2 = 10 s) ECD using solution contained 100 mM $Zn(NO_3)_2$. The pH of the solution was about 4.3. The deposition temperature and time were set to 60 °C and 3 min, respectively, while the deposition area was fixed to 0.36 cm^2 by masking. The thickness of the ZnO film was about 1-2 μm. It should be noted that we cannot deposit SnS on ZnO because ZnO is easily dissolved in the SnS deposition solution.

An indium electrode was fabricated by vacuum evaporation on the top film for the current density-voltage (J-V) measurement. The size of the electrode is 1 mm^2 and the distance between electrodes is 1 mm. The J-V characteristics were also characterized under 100 mW/cm^2 (AM1.5) irradiation using a solar simulator as the radiation source. Usually, the light is incident on the window-layer side, but we were not able to deposit transparent electrode on ZnO. Thus, the heterostructure was irradiated on the ITO glass (SnS) side.

3.3 Results and discussion

Elemental composition for the deposited SnS films is shown in Fig. 3.1 [15]. The increase in tartaric acid concentration resulted in sulfur increment and oxygen decrement. SnS deposited with 100 mM tartaric acid was selected for the ZnO/SnS heterostructure fabrication since no further reduction of oxygen content occurred for larger tartaric acid concentrations.

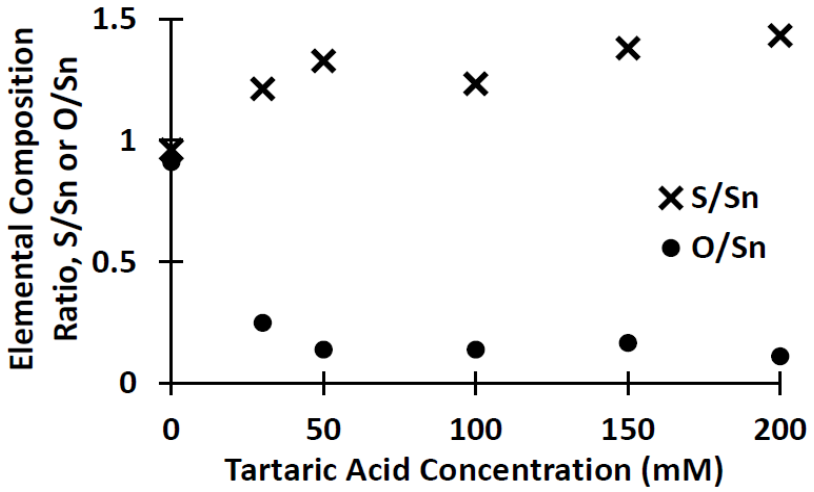

Fig. 3.1 Compositional analysis for SnS deposited with different concentrations of tartaric acid.

Figure 3.2 shows the measured optical transmittance for the deposited SnS samples. For SnS deposited without tartaric acid, no clear absorption edge observed, and the transmittance is low even in the infrared range, which corresponds to photon energies below the band gap. With 100 mM tartaric acid, the transmittance was increased, and the absorption edge became clearer. This indicates that defect states causing below-band-gap absorption were decreased by addition of tartaric acid.

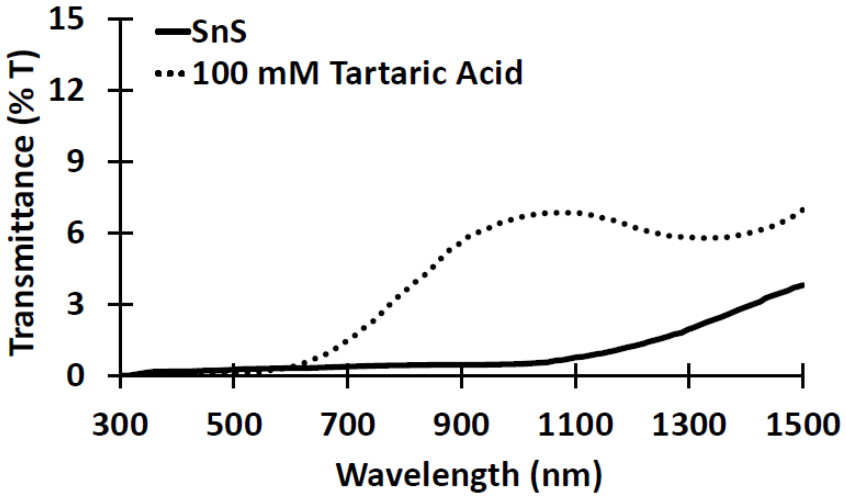

Fig. 3.2 Optical transmittance of the SnS films deposited with and without 100 mM tartaric acid.

Figure 3.3 depicts XRD results for the ZnO/SnS heterostructures. For both samples, several diffraction peaks of SnS and ZnO are observed, and thus both the SnS and ZnO layers in the heterostructures are poly-crystalline. The largest peak at 2Θ = 31.7º can be attributed to overlap of SnS (111) and ZnO (100) peaks. Sn-S impurity phases (SnS_2, Sn_2S_3) were not detected. With 100 mM tartaric acid, an additional SnS peak appeared at 2Θ = 39º. This would be due to the larger thickness and/or better crystallinity of the film deposited with tartaric acid.

Surface and cross-sectional SEM images of the ZnO/SnS heterostructures are shown in Fig. 3.4. Larger size of ZnO grains was observed when 100 mM tartaric acid was used for the SnS deposition. It was shown that the addition of 100 mM tartaric acid resulted in dense agglomerated surface grains of SnS [15]. This would in turn influence the morphology of the ZnO layer deposited on the SnS layer. In the cross sectional images, there is no clear interface between SnS and ZnO films for both the heterostructures. Thus, the hetero interface is formed between SnS and ZnO grains of various sizes, and many grain boundaries are included in the interface region.

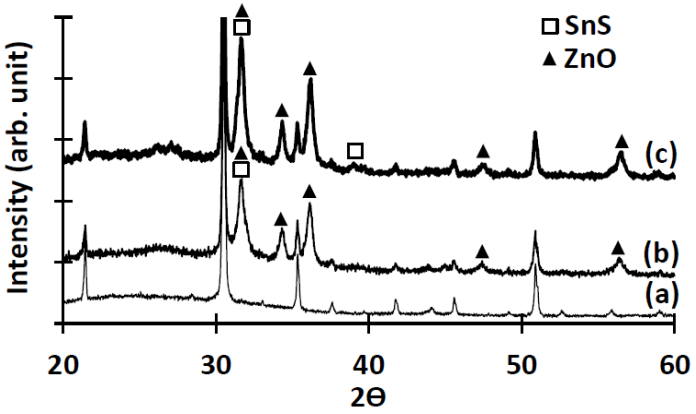

Fig. 3.3 XRD patterns for the measured samples (a) the ITO substrate, (b) ZnO/SnS (control), and (c) ZnO/SnS with 100 mM tartaric acid.

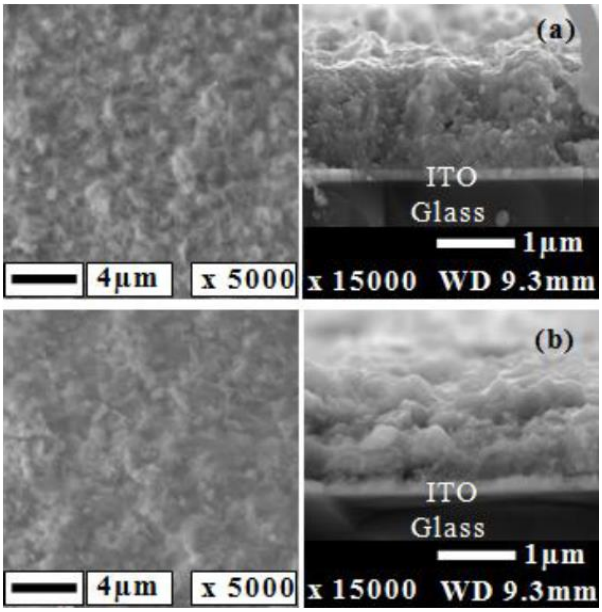

Fig. 3.4 Left: Surface morphology (x5000), and right: cross-sectional images (x15000) for the ZnO/SnS heterostructures fabricated (a) without and (b) with 100 mM tartaric acid.

Figure 3.5 illustrates the J-V characteristics of the heterostructures in the dark and under AM1.5 illumination. The fabricated heterostructures show clear rectifying property with some leakage current. This leakage might be associated with many grain boundaries at the interface as shown in the cross sectional SEM images (Fig. 3.4), which may act as a leakage path. Under AM1.5 irradiation shown by the expanded

curves in Figs. 3.5(b) and 3.5(c), both the heterostructures exhibited very weak photovoltaic properties: the open circuit voltage was less than 0.01 V and the short-circuit current density less than 1 μA/cm^2. The small output was partly due to the fact that the cell was irradiated on the SnS side. Carriers were photo-generated near the SnS/ITO interface, and majority of them cannot reach the p-n junction (the ZnO/SnS interface). Still, a larger output could be expected if the SnS layer and the interface have sufficiently high quality. With addition of tartaric acid, the oxygen content in the SnS film decreases as shown in Fig. 3.1, and the optical transmittance in the infrared range significantly increased as shown in Fig. 3.2. However, those improvements in the film quality did not lead to improvement of solar cell performance. This indicates that the poor photovoltaic properties of ECD ZnO/SnS heterostructures will be due to interface properties rather than those of bulk of the SnS layer.

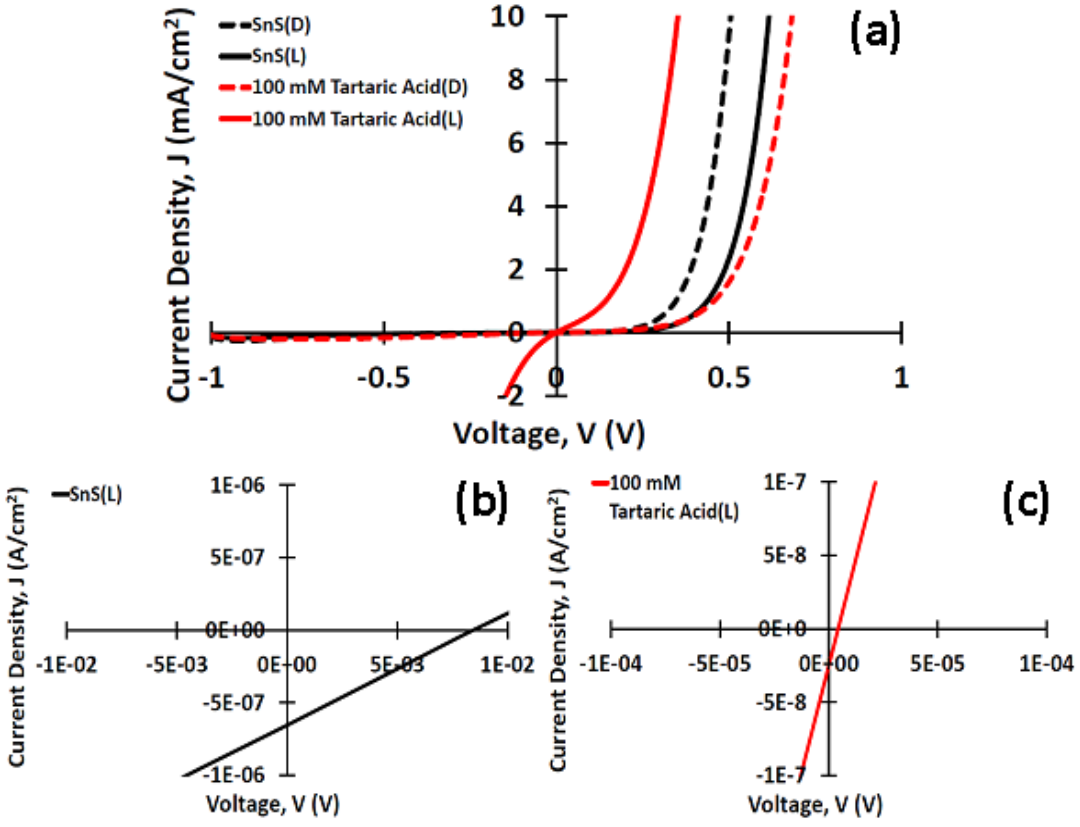

Fig. 3.5 J-V measurement for ZnO/SnS heterostructures: (a) in the dark, (D) and under AM 1.5 irradiation, (L); expanded curves for AM 1.5 (b) SnS, and (c) 100 mM tartaric acid.

3.4 Conclusion

ZnO/SnS heterostructures have been fabricated by ECD. To improve the SnS film properties, tartaric acid was introduced as a complexing agent into the deposition solution. The deposition with 100 mM tartaric acid resulted in larger optical transmittance and smaller oxygen content. ZnO was deposited on SnS by two steps pulse ECD. Both the heterostructures fabricated with/without tartaric acid showed clear rectifying properties. However, photovoltaic properties were not improved by the addition of tartaric acid.

References

[1] K. T. Ramakrishna Reddy, P. Purandhara Reddy, P. K. Datta, and R. W. Miles, Thin Solid Films 403-404 (2002) 116-119.

[2] H. Noguchi, A. Setiyadi, H. Tanamura, T. Nagatomo, and O. Omoto, Sol. Energy Mater. Sol. Cells 35 (1994) 325-331.

[3] B. Ghosh, M. Das, P. Banerjee, and S. Das, Sol. Energy Mater. Sol. Cells 92 (2008) 1099-1104.

[4] M. Ristov, G. Sinadinovski, M. Mitreski, and M. Ristova, Sol. Energy Mater. Sol. Cells 69 (2001) 17-24.

[5] B. Ghosh, M. Das, P. Banerjee, and S. Das, Semicond. Sci. Technol. 24 (2009) 025024.

[6] N. Koteswara Reddy and K. T. Ramakrishna Reddy, Thin Solid Films 325 (1998) 4-6.

[7] T. Ikuno, R. Suzuki, K. Kitazumi, N. Takahashi, N. Kato, and K. Higuchi, Appl. Phys. Lett. 102 (2013) 193901.

[8] S. Chang, K. Ishikawa, and M. Sugiyama, Thin Solid Films 589 (2015) 408-411.

[9] M. Ichimura and H. Takagi, Jpn. J. Appl. Phys. 47 (2008) 7845-7847.

[10] M. Gunasekaran and M. Ichimura, Sol. Energy Mater. Sol. Cells 91 (2007) 774-778.

[11] S. Cheng, Y. He, and G. Chen, Mater. Chem. Phys. 110 (2008) 449-453.

[12] S. Cheng, Y. He, G. Chen, E.-C. Cho, and G. Conibeer, Surf. Coat. Technol. 202 (2008) 6070-6074.

[13] J. R. Brownson, C. Georges, G. Larramona, A. Jacob, B. Delatouche, and C. Lévy-Clément, J. Electrochem. Soc. 155 (2008) D40-D46.

[14] F. Kang and M. Ichimura, Thin Solid Films 519 (2010) 725-728.

[15] A. Supee, Y. Tanaka, and M. Ichimura, Mater. Sci. Semicond. Process. 38 (2015) 290-297.

Chapter 4

Effects of complexing agents on electrochemical deposition of FeS_xO_y thin films

4.1 Introduction

Complexing agents are commonly used in solution deposition processes, and they are expected to improve the electrolyte stability, produce sufficient adherence, and smooth microstructure. For the CBD process, Vedavathi et al. found that FeS_2 films deposited using 0.1 M ethylenediaminetetraacetic (acid-EDTA) and 10-14 M ammonia were crystalline and that with 14 M ammonia, a pure pyrite phase with better surface morphology and lower film resistivity was obtained [1]. Kassim et al. [2] concluded that by increasing sodium tartrate concentration (0.1-0.3 M), the number of FeS peaks in the X-ray diffraction results was reduced, the absorbance as well as the number of grains decreased. In the successive ionic layer adsorption and reaction method, Manikandan et al. [3] claimed that the triethanolamine presence in the precursor solution resulted in a hexagonal shape of the crystalline structure in FeS_2 films.

So far, there is no work reported on the effects of complexing agents in iron sulfide films deposited by ECD. Thus, we carried out the ECD of iron sulfide under different concentrations of tartaric acid ($C_4H_6O_6$) and lactic acid [$CH_3CH(OH)COOH$]. Both chemicals have been successfully used to control the composition and morphology in the ECD of sulfides [4-6]. In our previous work, it was shown that as-deposited iron sulfide films were amorphous and included significant amounts of oxygen [7]. Thus, the deposit is denoted as FeS_xO_y. The FeS_xO_y film deposited without complexing agents was set as the control sample, and the effects of different concentrations of complexing agents were investigated in terms of cyclic voltammetry, thickness, surface morphology, composition ratio, crystallinity, optical transmittance, and photoresponse. As shown below, the oxygen content in the deposited films was significantly reduced by adding the complexing agents. We discuss the influence of oxygen on the properties of iron sulfide by comparing the control FeS_xO_y sample and the films deposited with the complexing agents.

4.2 Experiments

ECD was performed in the galvanostatic (I = -2.0 mA/cm^2) mode at 15 ºC for 1.5 min. The deposition and PEC setup, as well as film characterization were similar to those explained in chapter 2. The basic electrolyte solution contained 100 mM $Na_2S_2O_3$ and 30 mM $FeSO_4$ for the control sample [7], and different concentrations of tartaric acid (5-50 mM), and lactic acid (56-167 mM) were added to the basic solution as the complexing agents. Similar selection concept as chapter 2 was applied for the concentration of complexing agents. However, for the lactic acid, only high concentrations were used because the acid is in liquid form and the minimum measurement scale in basic pipette was not small enough for the lower concentration ranges. The solution pH was maintained at about 4.3-4.8 by using NH_4OH. After the ECD process was completed, the deposited film was immediately dried with N_2 gas. A xenon lamp (100 mW/cm^2) was applied in the PEC measurements.

In this galvanostatic deposition of FeS_xO_y with complexing agents, the chemical addition initially begins with $Na_2S_2O_3$ and then $FeSO_4$. The complexing agents used in this research are basically acidic and by introducing them after the $FeSO_4$ addition, the pH dropped and the colour of the solution changed from clear to white cloudy. Thus, NH_4OH was considered for maintaining the pH as close as to the basic electrolyte solution. However, with a few drops of NH_4OH after the $FeSO_4$ addition, the black layer appeared on top of the solution and by stirring, the colour of the solution completely changed into black/dark. Obviously, with the colour changing, the undesired chemical reaction occurred. By considering all the possibility of chemical sequences, the sequence then started with the complexing agents, followed by NH_4OH, $Na_2S_2O_3$ and lastly $FeSO_4$ whereby the appearance of the solution almost similar as basic electrolyte solution.

4.3 Results and discussion

Figure 4.1 illustrates the results of CV for the FeS_xO_y deposition solution with and without complexing agents. All the samples showed clear anodic and cathodic peaks, and during the initial scan from 0 V to about -0.9 V, no visible negative current

appeared. The cathodic current started to increase at about -0.9 V. For the control sample and samples with a low concentration of tartaric acid (10 mM), small shifts in the cathodic peaks were observed with similar cathodic current density and curve shapes. Meanwhile, for high concentrations of tartaric acid (50 mM) and lactic acid (56 and 111 mM), even though the curve shapes seem similar, a larger negative current density was obtained. Thus, it can be concluded that the negative current was enhanced by the addition of high concentrations of tartaric acid and lactic acid in the FeS_xO_y deposition solution.

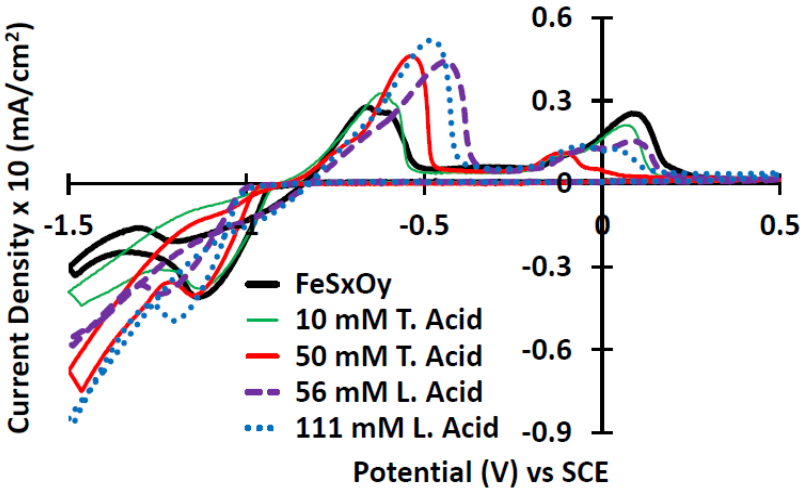

Fig. 4.1 CV for the solutions with and without the complexing agents, tartaric acid (T. acid) and lactic acid (L. acid).

Figure 4.2 summarizes the thickness measured for the deposited samples. The films fully covered the targeted deposition area. Overall, the thickness was increased with the addition of the complexing agents. For the deposition with tartaric acid, the thickness was increased once, then decreased at 30 mM, and increased again with increasing concentration. The reason for such oscillation behavior is not yet understood.

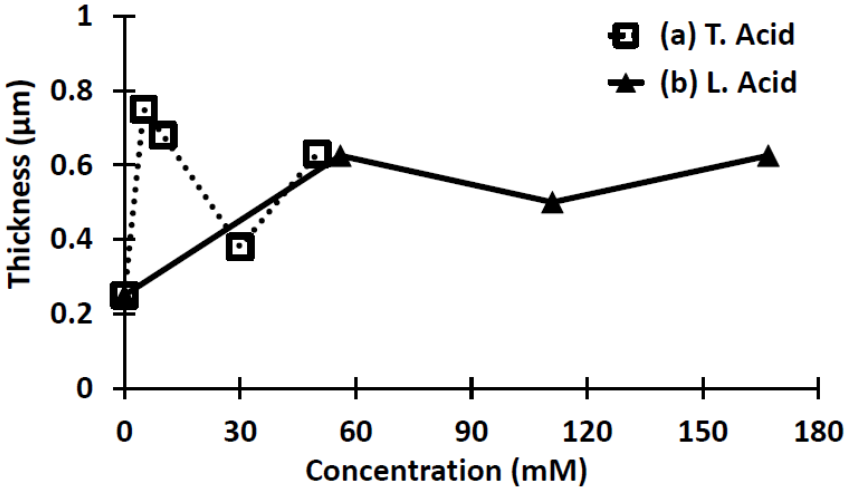

Fig. 4.2 Thickness of the deposited films as a function of the complexing agent concentration: (a) tartaric acid (T. acid) and (b) lactic acid (L. acid).

Figures 4.3(a)-4.3(f) shows the SEM images for the selected samples. The FeS_xO_y control sample exhibited an inhomogeneous grain distribution of various grain sizes. The increase in the tartaric acid concentration from 5 to 10 mM resulted in homogeneous smaller grain sizes with clear grain boundaries, as shown in Figs. 4.3(b) and 4.3(c). Similar effects on surface morphology were obtained with increasing lactic acid concentration [Figs. 4.3(e) and 4.3(f)]. Clearly, with both acids used as the complexing agents in the solution, the grains size was reduced and the film uniformity was improved.

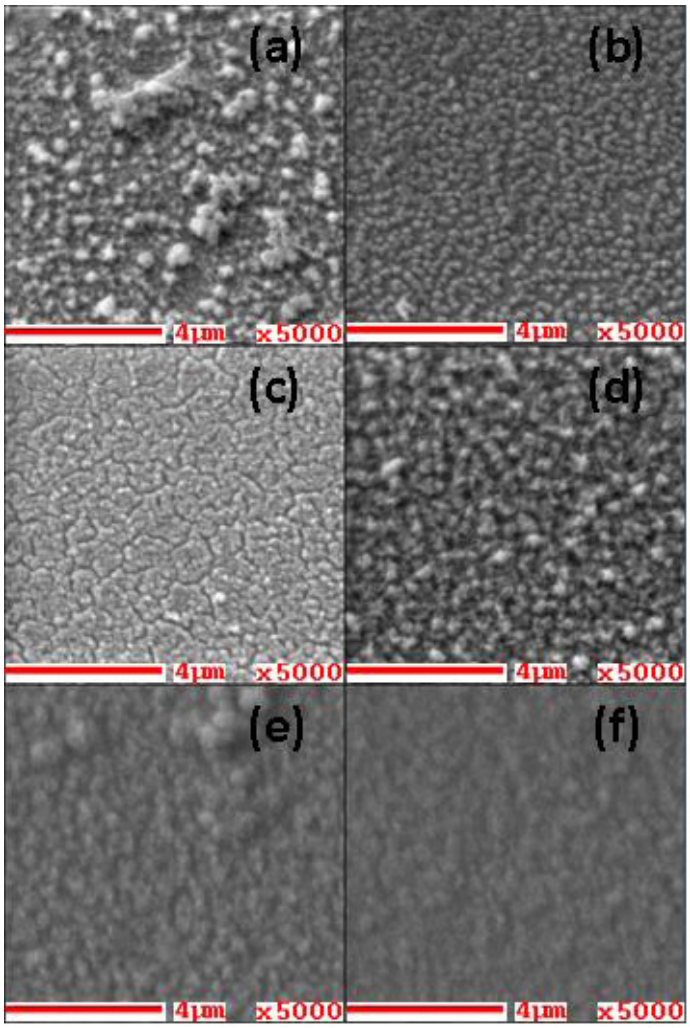

Fig. 4.3 SEM images for selected deposited samples (Scale bar: 4 µm, x5000): (a) control FeS_xO_y, (b) tartaric acid 5 mM, (c) tartaric acid 10 mM, (d) tartaric acid 30 mM, (e) lactic acid 56 mM, and (f) lactic acid 111 mM.

Auger electron spectroscopy (AES) results for the selected samples are shown in Fig. 4.4. S/Fe and O/Fe ratios were calculated using the commercially available standard chemicals FeS and Fe_2O_3 as the reference and are plotted in Figs. 4.5(a) and 4.5(b). Similar approaches as chapter 2 were used in the ratio calculation. For the FeS_xO_y film deposited with tartaric acid, as shown in Fig. 4.5(a), the S/Fe ratio was once decreased and then increased with increasing tartaric acid concentration. Thus there is no clear tendency of increase or decrease in the S/Fe ratio with the addition of tartaric acid. The reason for the decrease in the S/Fe ratio when the tartaric acid

concentration is low is not yet understood. The S/Fe ratio is equal to about 2 with some residue amount of oxygen for the sample with 30 mM tartaric acid. The S/Fe ratio was also almost constant for the films deposited with lactic acid, as depicted in Fig. 4.5(b), even though the lactic acid concentration was increased.

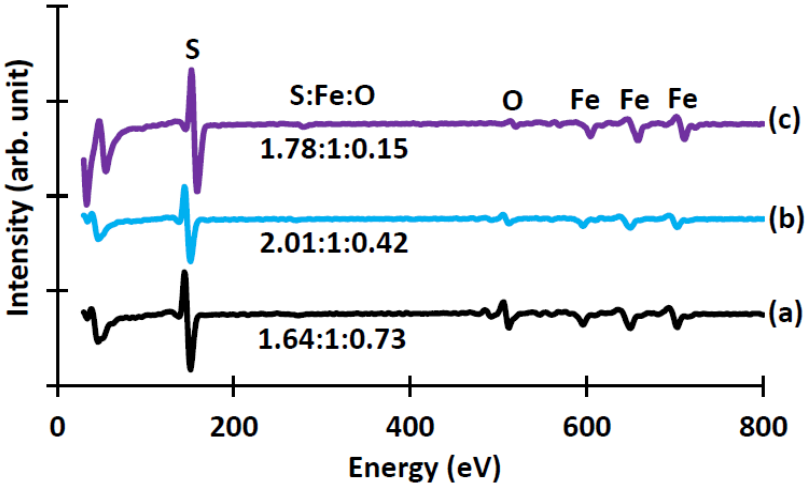

Fig. 4.4 AES spectra for selected samples: (a) control FeS_xO_y, (b) tartaric acid 30 mM, and (c) lactic acid 56 mM.

On the other hand, the oxygen content in FeS_xO_y film was strongly affected by the concentrations of complexing agents. For the tartaric acid samples, as shown in Fig. 4.5(a), the O/Fe ratio was significantly reduced at concentrations > 10 mM. Further increase in the concentration up to 50 mM resulted in further reduction in the oxygen content. For the lactic acid samples also, the O/Fe ratio was greatly reduced when 56 mM lactic acid was added to the deposition solution. However, no further reduction occurred for concentrations greater than 56 mM.

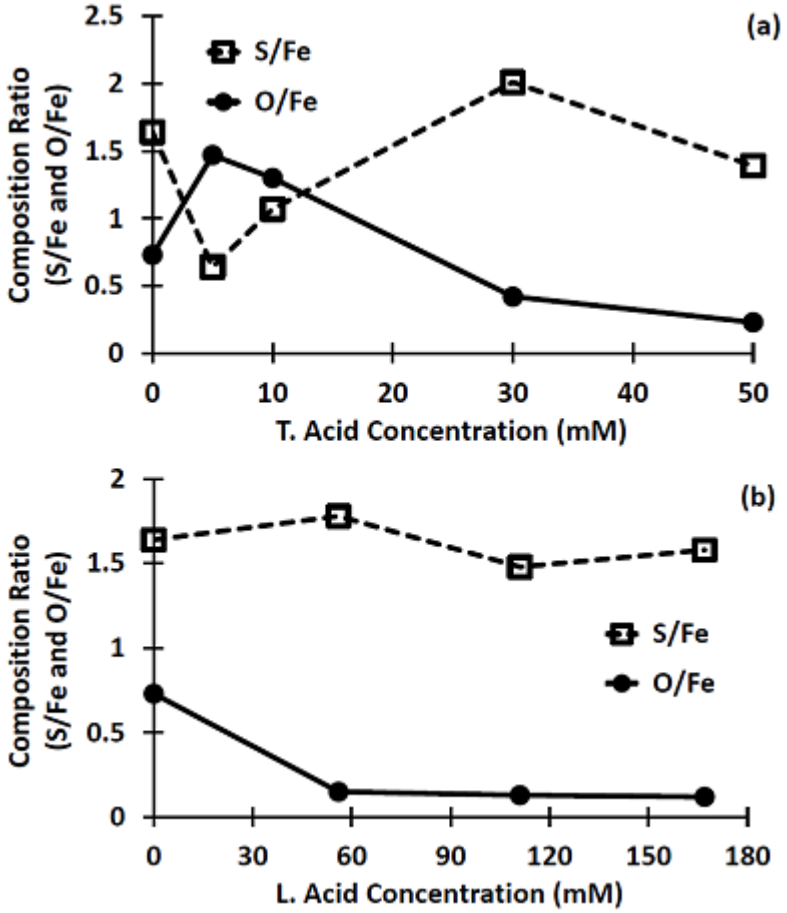

Fig. 4.5 Compositional analysis by AES for the deposited samples with different concentrations of the complexing agents: (a) tartaric acid (T. acid) and (b) lactic acid (L. acid).

The XRD patterns measured for selected deposited samples and ITO are shown in Fig. 4.6. All the observed diffraction peaks are attributed to ITO regardless of the types of complexing agents and the concentration. Thus the deposited films are amorphous, regardless of whether the complexing agents were used.

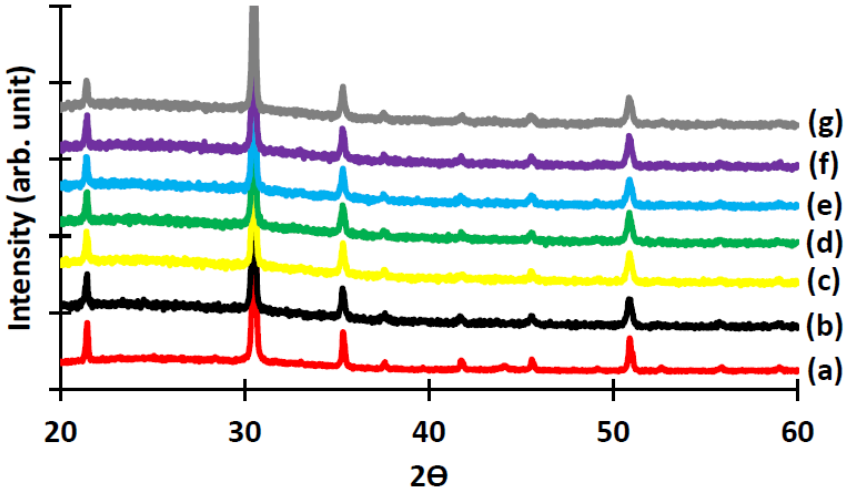

Fig. 4.6 XRD patterns for selected deposited samples: (a) ITO, (b) control FeS_xO_y, (c) tartaric acid 5 mM, (d) tartaric acid 10 mM, (e) tartaric acid 30 mM, (f) lactic acid 56 mM, and (g) lactic acid 111 mM.

Figure 4.7 represents the Raman spectra for the films deposited under different concentrations of complexing agents. Raman peaks were formerly reported as follows: pyrite: 336, 341, 373, 377, 425 cm^{-1} [8-9]; marcasite: 319, 324, 382 cm^{-1} [8-9]; FeS_xO_y: 249, 305 cm^{-1}; and mackinawite ($Fe_{1+x}S$): 208, 256, 298 cm^{-1} [10]. For the measured samples, the $Fe_{1+x}S$ peak appeared only in the control and 56 mM lactic acid samples, while no FeS_xO_y phase was observed with a low tartaric acid concentration (10 mM). At high concentrations of tartaric acid (30-50 mM) and lactic acid (56-111 mM), an additional pyrite peak appeared at around 375 cm^{-1}. The highest marcasite peak intensity (326 cm^{-1}) was found for the sample deposited with 50 mM tartaric acid.

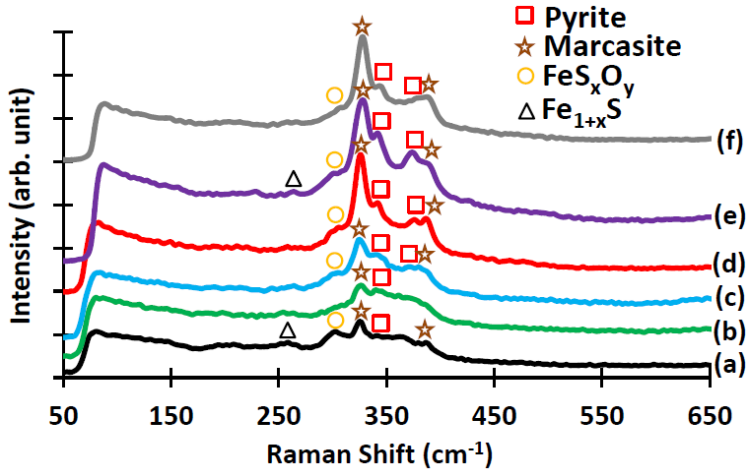

Fig. 4.7 Raman spectra for deposited samples: (a) control FeS_xO_y, (b) tartaric acid 10 mM, (c) tartaric acid 30 mM, (d) tartaric acid 50 mM, (e) lactic acid 56 mM, and (f) lactic acid 111 mM.

Figure 4.8 illustrates the optical in-line transmittance of the deposited samples. The deposited films with tartaric acid exhibit transmittance comparable to that of the control sample, and a clear absorption edge was observed for the control and 30 mM tartaric acid samples. However, no clear absorption edge was detected and lower transmittance (< 2%) was obtained with lactic acid addition. The low transmittance is partly a result of the scattering due to the surface roughness.

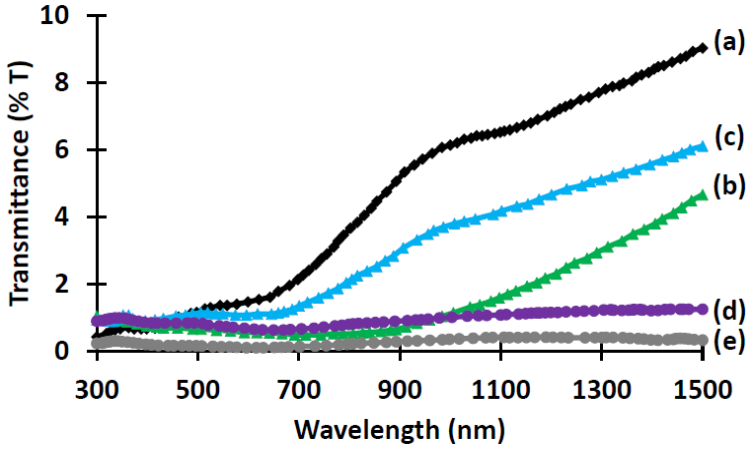

Fig. 4.8 Optical in-line transmittance of deposited samples: (a) control FeS_xO_y, (b) tartaric acid 10 mM, (c) tartaric acid 30 mM, (d) lactic acid 56 mM, and (e) lactic acid 111 mM.

To estimate the band gap, we plotted $(\alpha h\nu)^2$ and $(\alpha h\nu)^{1/2}$ vs. hν, where α is the absorption coefficient and hν is the photon energy. Examples of the plots are shown in Figs. 4.9(a) and 4.9(b). The plot of $(\alpha h\nu)^{1/2}$ in Fig. 4.9(b) does not have a clear linear portion, while in the plot of $(\alpha h\nu)^2$ depicted in Fig. 4.9(a), extrapolations of the linear part would intersect the x-axis at approximately between 1−1.2 eV.

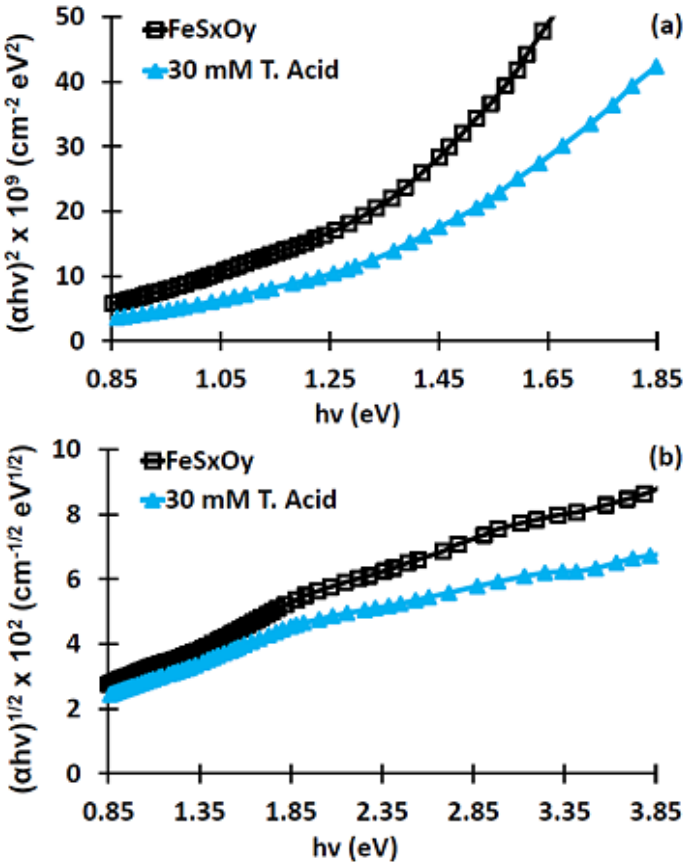

Fig. 4.9 Plots of (a) $(\alpha h\nu)^2$ and (b) $(\alpha h\nu)^{1/2}$ versus hν for deposited samples.

Figure 4.10 depicts the photocurrent response in the PEC measurement for the deposited samples. The weak photoresponse was observed for the control sample, and samples with high concentrations of tartaric acid (30-50 mM) and lactic acid (56-111 mM) only in negative potential scans. The negative current increased as the sample was illuminated (on), and then decreased as the illumination was interrupted (dark-off). In the PEC measurement, the current due to the minority carrier was enhanced, thus, the results showed that the samples can be classified as p-type.

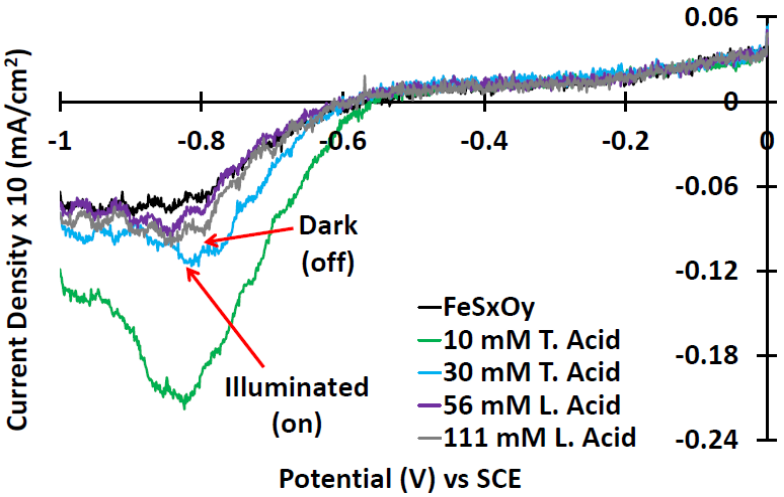

Fig. 4.10 Photocurrent responses in the PEC measurement for the control sample and the samples deposited with tartaric acid (T. acid) and lactic acid (L. acid).

Complexing agents are normally used to avoid precipitation (e.g., metal hydroxide) as they slow down the release rate of metallic ions in electrolyte solution as a result of metal complex formation. In this work, the oxygen content in the deposited films was significantly reduced at high concentrations of tartaric acid (> 10 mM) and lactic acid (56-167 mM). Oxygen is probably included in the film initially as $Fe(OH)_2$, and then decomposed into iron oxides. For both complexing agents, the concentration of free Fe^{2+} ions in the solution would be decreased owing to the formation of some iron complex species that retarded the release of free Fe^{2+} ions and consequently suppressed the formation of $Fe(OH)_2$. Therefore, both complexing agents seem to retard oxide formation. On the other hand, the film thickness was increased with the addition of the complexing agents. The deposition in this work is galvanostatic, i.e., the electrical charge supplied was constant for all the depositions. Thus, a part of the current was consumed for reactions other than the sulfide formation without the complexing agents, and the complexing agents suppress such superfluous reactions and increase the film thickness. In our previous works, it was suggested that tartaric acid enhances the reduction of the sulfur species in ECD of SnS [6]. For FeS_xO_y, although the S/Fe ratio did not increase significantly, the complexing agents are considered to enhance the reduction of the sulfur species and the sulfide formation, resulting in the increase in the film thickness.

The addition of the complexing agents also resulted in higher marcasite peak intensity in the Raman spectra. In addition, lactic acid in the solution results in poor transmittance of less than 2%. This low transmittance is partly due to the larger film thickness and partly associated with the defect states that cause below-band-gap absorption and/or the marcasite phase, which has a much smaller band gap. In PEC measurement, no improvement of the photoresponse was observed for the samples deposited with the complexing agents. Thus, although the composition became more stoichiometric with greatly reduced oxygen content upon the addition of the complexing agents, the optical and electrical properties do not seem to be significantly improved. In other words, the properties of amorphous iron sulfide are not seriously deteriorated by the introduction of oxygen. The results of a Mössbauer study have shown that Fe atoms are coordinated to six anions (S or O) in ECD-deposited amorphous FeS_xO_y, as in crystalline FeS_2 [11]. Thus, in spite of the dissimilarity of iron sulfides and iron oxides, sulfur and oxygen seem to play a similar anionic role in amorphous FeS_xO_y. As a result, its properties are not drastically influenced by changes in the oxygen content.

In future studies, heterostructures with an n-type semiconductor, such as ZnO, will be fabricated using FeS_xO_y films deposited with the complexing agents, and the effects of film composition (oxygen content) on the junction properties will be discussed.

4.4 Conclusion

FeS_xO_y thin films were deposited on ITO-coated glass substrates via galvanostatic ECD from an aqueous solution containing $Na_2S_2O_3$ and $FeSO_4$ with controlled pH, and the effects of different concentrations of tartaric acid and lactic acid were studied. With the addition of complexing agents, the thickness was increased, and the O/Fe ratio was decreased. However, no significant effects were found for photoresponse and crystallinity. Thus, oxygen atoms seem not to significantly affect the properties of amorphous iron sulfide films, probably because the local bonding configuration around Fe atoms is not altered by the substitution of sulfur with oxygen. The reduction in the oxygen content in the FeS_xO_y film can be explained by considering the suppression of $Fe(OH)_2$ formation.

References

[1] A. Vedavathi, K. T. Ramakrishna Reddy, and Y. Munikrishna Reddy, IOSR J. Eng. 05 (2015) 65-70.

[2] A. Kassim, H. S. Min, L. Y. Yee, T. W. Tee, and S. Nagalingam, Can. J. Pure Appl. Sci. 6 (2012) 1863-1867.

[3] K. Manikandan, P. Mani, C. Surendra Dilip, S. Valli, P. Fermi Hilbert Inbaraj, and J. Joseph Prince, Appl. Surf. Sci. 288 (2014) 76-82.

[4] F. Kang and M. Ichimura, Thin Solid Films 519 (2010) 725-728.

[5] J. R. Brownson, C. Georges, G. Larramona, A. Jacob, B. Delatouche, and C. Lévy-Clément, J. Electrochem. Soc. 155 (2008) D40-D46.

[6] A. Supee, Y. Tanaka, and M. Ichimura, Mater. Sci. Semicond. Process. 38 (2015) 290-297.

[7] S. Kawai, R. Yamazaki, S. Sobue, E. Okuno, and M. Ichimura, APL Mater. 2 (2014) 032110.

[8] M. Umehara, Y. Takeda, H. Azuma, and T. Motohiro, Jpn. J. Appl. Phys. 51 (2012) 02BP10.

[9] R. Morrish, R. Silverstein, and C. A. Wolden, J. Am. Chem. Soc. 134 (2012) 17854-17857.

[10] J. A. Bourdoiseau, M. Jeannin, R. Sabot, C. Rémazeilles, and P. Refait, Corros. Sci. 50 (2008) 3247-3255.

[11] M. Ichimura, T. Kajima, S. Kawai, and K. Mibu, Jpn. J. Appl. Phys. 55 (2016) 038006.

Chapter 5

Effects of complexing agents on electrochemical deposition of FeS_xO_y in ZnO/FeS_xO_y heterostructures

5.1 Introduction

In our work [1], tartaric acid ($C_4H_6O_6$) and lactic acid [$CH_3CH(OH)COOH$] were used as the complexing agents in galvanostatic electrochemical deposition (ECD) of FeS_xO_y. Addition of complexing agents in FeS_xO_y deposition solution resulted in larger film thickness and reduced oxygen content in the films.

In previous works of Fe-S based heterostructures, the ZnO/FeS_2 heterostructures fabricated by Wang et al. only show rectification properties with no photovoltaic effects [2]. Similar phenomena also occurred for the others in their fabricated ZnO/Fe-S-O heterostructures [3-4]. Nevertheless, there are no report on the heterostructures based on ECD FeS_xO_y deposited with a complexing agent. Thus, we further implement our previous condition of FeS_xO_y ECD with 30 mM tartaric acid and 56 mM lactic acid in ZnO/FeS_xO_y heterostructure fabrication. ZnO was selected as window layer material and it was deposited by two steps pulse ECD [5]. Since both the FeS_xO_y and ZnO are abundant and non-toxic elements, the ZnO/FeS_xO_y heterostructure is expected to be well suited for low-cost solar cells applications. A heterostructure with FeS_xO_y fabricated without complexing agents was set as a control sample, and the effects of complexing agents in term of oxygen content in the FeS_xO_y films towards the heterostructure properties were investigated.

5.2 Experiments

The film thickness measurement, X-ray diffraction (XRD), and elemental compositional analysis were conducted using the same equipment/method as mentioned in chapter 2. The deposition area and condition, as well as the pH adjustment (about 4.7-5.3) are the same as described in chapter 4. FeS_xO_y films without (control sample) or with the complexing agents (tartaric acid: 30 mM, and lactic acid: 56 mM) were

initially deposited on ITO. The thicknesses of the films were as follows: FeS_xO_y control (0.25 μm), FeS_xO_y with complexing agents: 30 mM tartaric acid (0.38 μm), 56 mM lactic acid (0.63 μm). The techniques elaborated in chapter 3 were adopted for the ZnO deposition on FeS_xO_y film, indium evaporation, and current density-voltage (J-V) measurement. The thickness of the ZnO film was about 1-2 μm. The pH of the ZnO deposition solution was about 4.6. It should be noted that if ZnO was deposited first, the ZnO film would be dissolved during the subsequent FeS_xO_y deposition process [3]. Thus, FeS_xO_y was deposited on the ITO substrate first, and the heterostructure was irradiated on the ITO glass (FeS_xO_y) side in the J-V measurement under AM1.5.

5.3 Results and discussion

Elemental composition for the deposited FeS_xO_y films is shown in Figs. 5.1(a) and 5.1(b) [1]. There is no clear tendency of increase or decrease in S/Fe ratio with increasing tartaric acid concentration as depicted in Fig. 5.1(a). Meanwhile, for the lactic acid samples as shown in Fig. 5.1(b), the S/Fe ratio was almost constant regardless of concentrations. On the other side, the oxygen content in the FeS_xO_y films was significantly reduced at concentrations ≥ 30 mM for tartaric acid [Fig. 5.1(a)], and ≥ 56 mM for lactic acid samples [Fig. 5.1(b)]. Thus, FeS_xO_y deposited with 30 mM tartaric acid and 56 mM lactic acid were selected for the ZnO/FeS_xO_y heterostructures fabrication since there is no drastic reduction of oxygen content with concentrations exceeding those above mentioned.

Figure 5.2 shows the measured optical in-line transmittance for the deposited FeS_xO_y samples. For the control and 30 mM tartaric acid samples, the transmittance is comparable with clear absorption edge was observed. Low transmittance even in the infrared range and no clear absorption edge was obtained with lactic acid sample, which would be partly associated to the larger film thickness, scattering due to the surface roughness, and also photo-absorption due to defect states. This indicates that the defect states were not reduced by addition of both the complexing agents.

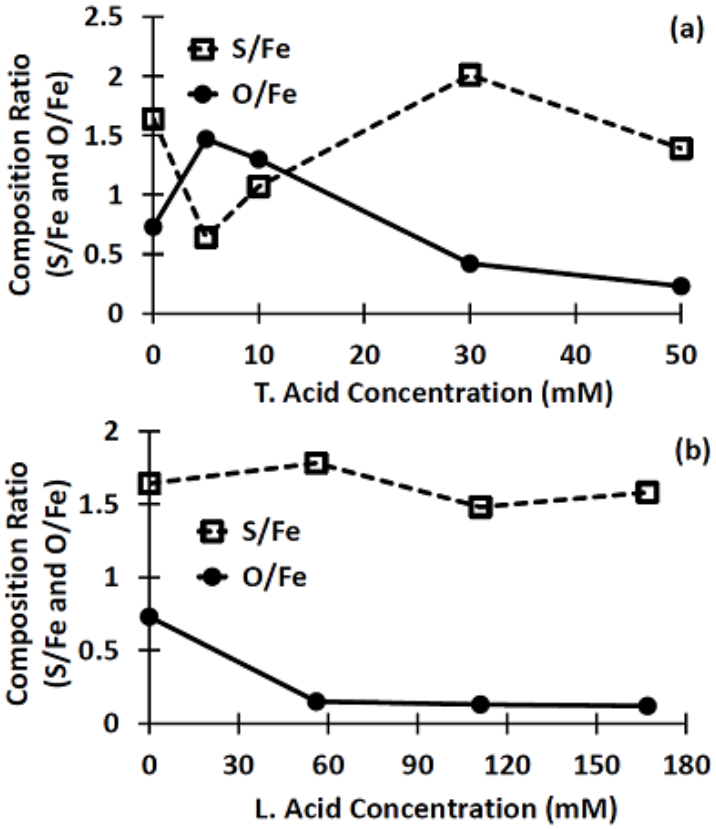

Fig. 5.1 Elemental compositional analysis for FeS_xO_y deposited with different concentrations of complexing agents: (a) tartaric acid (T. acid) and (b) lactic acid (L. acid) [1].

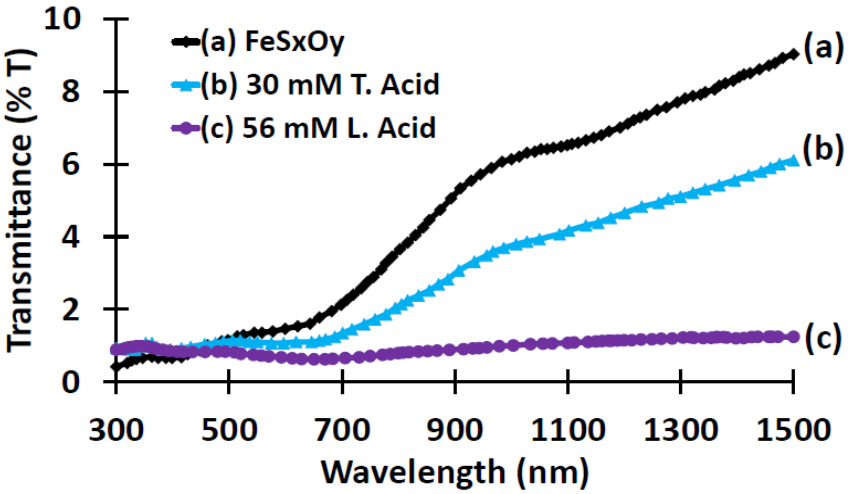

Fig. 5.2 Optical in-line transmittance of the deposited FeS_xO_y films: (a) FeS_xO_y control, FeS_xO_y with (b) tartaric acid (T. acid), and (c) lactic acid (L. acid).

Figure 5.3 depicts an example of XRD results for the ZnO/FeS_xO_y heterostructure with lactic acid. Only ZnO peaks were appeared at 2Θ = 31.7, 34.4, 36.2, 47.5, and 56.4º. In our previous work, the XRD peaks of FeS_xO_y films deposited on ITO with/without complexing agents correspond to ITO peaks, and thus the films were classified as amorphous [1]. Thus the fabricated heterostructure consists of amorphous FeS_xO_y and poly-crystalline ZnO layers.

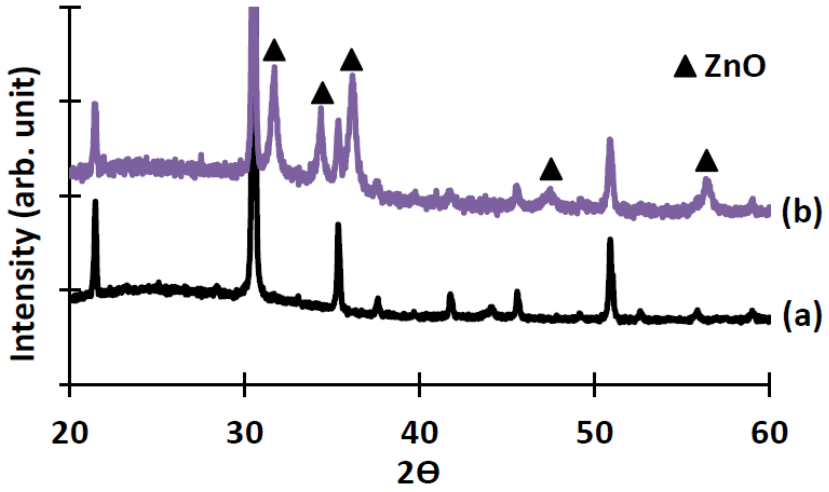

Fig. 5.3 XRD patterns for the measured samples: (a) the ITO substrate, and (b) ZnO/FeS_xO_y with 56 mM lactic acid.

Figure 5.4 illustrates the J-V characteristics of the heterostructures in the dark and under AM1.5 illumination. The fabricated heterostructures show rectifying property with significant large leakage current. Under AM1.5 irradiation, the heterostructures exhibited negligible photovoltaic properties. This was partly due to the fact that the carriers were photo-generated near the FeS_xO_y/ITO interface, and majority of them cannot reach the p-n junction (the ZnO/FeS_xO_y interface). In addition, our ZnO/FeS_xO_y interface may also contain a large number of trap states which restricted the mobility of the carriers across the p-n junction. Thus, the improvement of photovoltaic properties could be expected if the quality of the interface is sufficiently high.

With addition of both complexing agents, the oxygen content in the FeS_xO_y films were decreased as shown in Fig. 5.1. However, that oxygen reduction did not lead to improvement of solar cell performance. This indicates that the oxygen content in the

FeS_xO_y film has no influences towards the performance of the solar cell. This is probably because the local bonding configuration around Fe atoms is not altered by the substitution of sulfur with oxygen which results in insignificant improvement of optical and electrical properties of FeS_xO_y film [1]. Thus, poor photovoltaic properties of ECD ZnO/FeS_xO_y heterostructures could be attributed to the properties of the bulk FeS_xO_y layer as well as the interface layer.

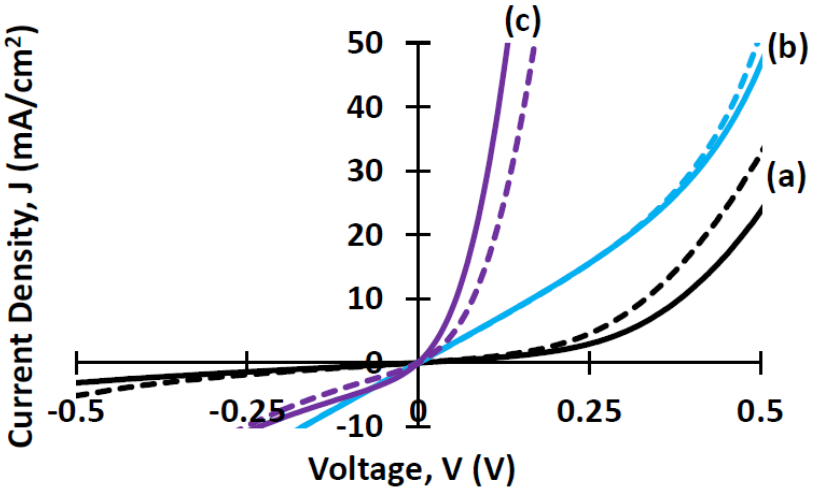

Fig. 5.4 J-V measurement for ZnO/FeS_xO_y heterostructures in the dark (dotted line) and under AM 1.5 irradiation (continuous line): (a) FeS_xO_y control, FeS_xO_y with (b) 30 mM tartaric acid, and (c) 56 mM lactic acid.

5.4 Conclusion

ZnO/FeS_xO_y heterostructures have been fabricated by ECD. To alter the FeS_xO_y film properties, tartaric acid and lactic acid were introduced as the complexing agents into the deposition solution. The deposition with both complexing agents resulted in larger films thickness and smaller oxygen content. ZnO was deposited on FeS_xO_y by two steps pulse ECD. The rectifying properties were confirmed for all the heterostructures either with/without complexing agents. However, photovoltaic properties were not improved by the reduction of oxygen content in the FeS_xO_y film.

References

[1] A. Supee and M. Ichimura, Jpn. J. Appl. Phys. 55 (2016) 081202.

[2] D. Y. Wang, Y. T. Jiang, C. C. Lin, S. S. Li, Y. T. Wang, C. C. Chen, and C. W. Chen, Adv. Mater. 24 (2012) 3415-3420.

[3] S. Kawai, R. Yamazaki, S. Sobue, E. Okuno, and M. Ichimura, APL Mater. 2 (2014) 032110.

[4] K. Yang, S. Kawai, and M. Ichimura, Thin Solid Films 573 (2014) 1-5.

[5] M. Ichimura and H. Takagi, Jpn. J. Appl. Phys. 47 (2008) 7845-7847.

Chapter 6

Three steps pulse electrochemical deposition of FeS_xO_y thin films and their characterization

6.1 Introduction

In our previous work, we used galvanostatic [1] and potentiostatic [2-4] ECD to deposit iron sulfide films, and they mostly contain significant amount of oxygen. Thus, the deposit is denoted as FeS_xO_y. In addition, our galvanostatic FeS_xO_y films show p-type photocurrent response, is completely black/opaque for visibility, and exhibits optical in-line transmittance less than 10% in the wavelength range of 300 nm to 1500 nm [1]. In this research, we firstly attempt to deposit FeS_xO_y films by three steps pulse ECD. For SnS films deposited by three steps pulse ECD, it was found that the surface morphology and photosensitivity of the films were highly improved [5]. To our knowledge, there are no reports on fabrication of FeS_xO_y films based on three steps pulse ECD. The three-step ECD process consists of the deposition step, the dissolution step, and the intermediate (equilibrating) step. In this work, we will introduce two different pulse wave forms with the intermediate potential V_2 variation. Then we will discuss the effects of three steps pulse ECD in term of cyclic voltammetry, thickness, surface morphology, composition ratio, crystallinity, optical in-line transmittance, and photocurrent response. We found that V_2 has significant impact especially on the optical properties of the films.

6.2 Experiments

The similar ECD setup, the electrode's cleaning, the deposition condition (pH: about 5.2-5.3, temperature: room, area: 1 x 1 cm^2), and the films characterization as mentioned in chapter 2 were applied. ECD was performed using periodic three steps pulse with V_2 manipulation under two different condition; condition A (potential shifts from negative to positive): V_1 = -1 V vs SCE, on t_1 = 10 s; V_2 = ranging from -0.4 V to -0.8 V, t_2 = 10 s; V_3 = 0 V, t_3 = 10 s; and condition B (potential shifts from positive to negative): V_1 = 0 V vs SCE, on t_1 = 10 s; V_2 = ranging from -0.4 V to -0.8 V, t_2 = 10 s;

V_3 = -1 V, t_3 = 10 s. The deposition solution contained 100 mM $Na_2S_2O_3$ and 15 mM $FeSO_4$. The total deposition time for both the conditions was fixed to 7 min.

6.3 Results and discussion

Figure 6.1 illustrates CV for the deposition solution. The CV shows clear anodic and cathodic peaks, and in the range of 0 V to about -0.8 V, there is no visible cathodic current appeared. The cathodic current started to increase at about -0.8 V. The first cathodic current peak appeared at about -1 V and the second anodic current peak (small) appeared at about -0.7 V. By considering the possibility that hydrogen evolution may occur at high negative potential values, we selected condition A: V_1 = -1 V for the first step potential for reduction (deposition), V_2 ranging from -0.4 V to -0.8 V as the intermediate step potential, and V_3 = 0 V for the third step potential (dissolution).

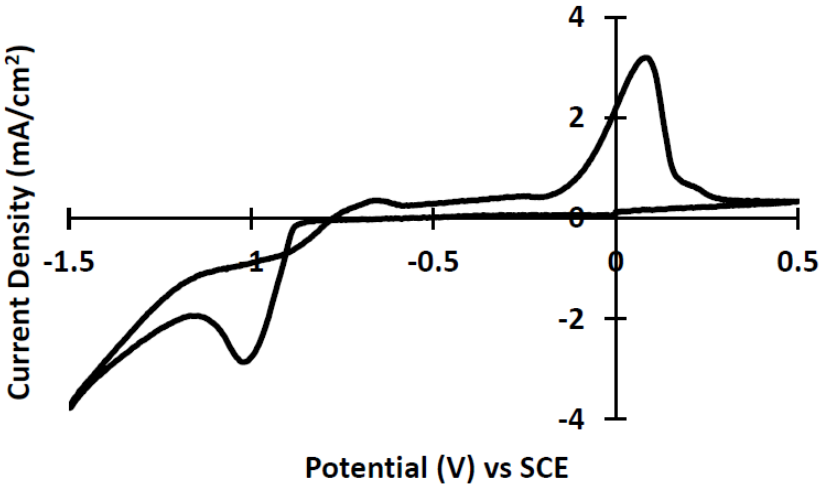

Fig. 6.1 Cyclic voltammetry for the FeS_xO_y deposition solution at room temperature.

The film thicknesses for condition A are about 0.12-0.14 µm, meanwhile for condition B are about 0.3-0.4 µm. Figures 6.2(a)-6.2(g) shows the SEM images for the samples. All the deposited films exhibit an inhomogeneous grain distribution consisting of various grain sizes. There is no specific patterns observed for the grain with V_2 variation for condition A. The film deposited under V_2 = -0.6 V [Fig. 6.2(b)] shows more dense morphology with relatively smaller grain size compared to Figs. 6.2(a) and 6.2(c). When the potential shifted from positive to negative (condition B), change in V_2

from -0.4 V to -0.8 V [Figs. 6.2(d)-6.2(f)] results in more dense morphology and more uniform shape and size of grain.

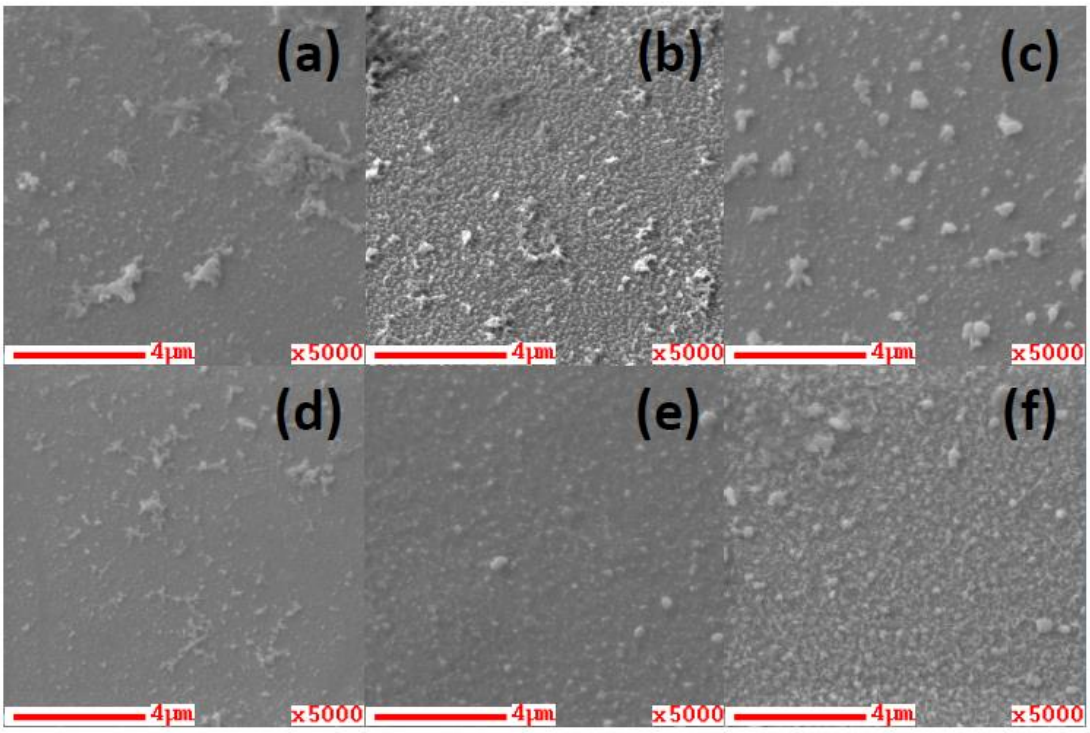

Fig. 6.2 SEM images for the samples (Scale bar: 4 μm, x5000): condition A (V_1 = -1 V, V_3 = 0 V), V_2: (a) -0.4 V, (b) -0.6 V, and (c) -0.8 V; condition B (V_1 = 0 V, V_3 = -1 V), V_2: (d) -0.4 V, (e) -0.6 V, and (f) -0.8 V.

Elemental composition ratios obtained by Auger electron spectroscopy (AES) for the samples are shown in Figs. 6.3(a) and 6.3(b). S/Fe and O/Fe ratios were calculated using the same method as in chapter 4. For the condition A, as depicted in Fig. 6.3(a), the S/Fe ratio was once increased and then decreased with more negative V_2 value. Thus there is no clear tendency of increase or decrease in the S/Fe ratio with V_2 variation. For the O/Fe ratio either, there are no significant effects when V_2 changed from -0.4 V to -0.8 V. On the other hand, the condition B as represented by Fig. 6.3(b) exhibits increment in the S/Fe and decrement in O/Fe ratios when the V_2 is more negative than -0.6 V.

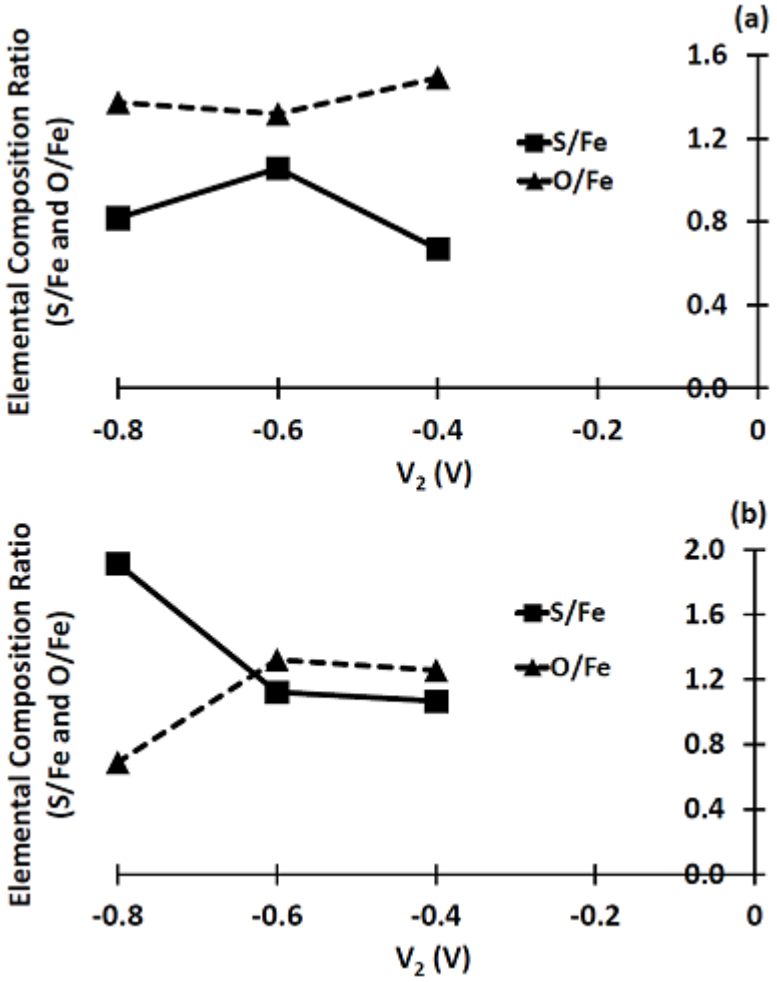

Fig. 6.3 Compositional analysis by AES for the deposited samples with V_2 variation: (a) condition A and (b) condition B.

Figure 6.4 represents the Raman spectra for the films. Raman peaks were formerly reported as follows: pyrite: 336, 341, 373, 377, 425 cm^{-1} [6-7]; marcasite: 319, 324, 382 cm^{-1} [6-7]; FeS_xO_y: 249, 305 cm^{-1}; and mackinawite ($Fe_{1+x}S$): 208, 256, 298 cm^{-1} [8]. For the measured samples as shown in Fig. 6.4, most of the peaks are correspond to marcasite (319 cm^{-1} and 326 cm^{-1}) and $Fe_{1+x}S$ (259 cm^{-1}). The FeS_xO_y peak appeared only for (f), condition B with V_2 = -0.8 V.

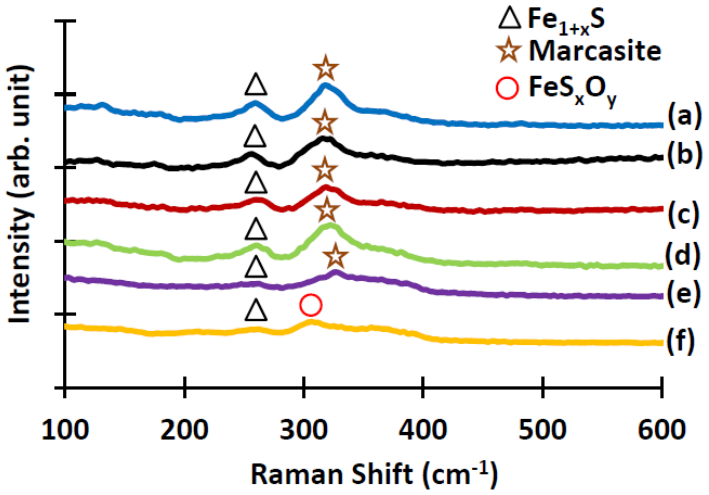

Fig. 6.4 Raman spectra for deposited samples: condition A , V_2: (a) -0.4 V, (b) -0.6 V, and (c) -0.8 V; condition B, V_2: (d) -0.4 V, (e) -0.6 V, and (f) -0.8 V.

Figure 6.5 shows an example of the XRD patterns measured for the sample deposited under condition A with V_2 = -0.6 V. All the observed XRD diffraction peaks are attributed to ITO. For all the other samples, we observed no diffraction peak attributed to the film, and thus the deposited films are considered as amorphous.

Figure 6.6 illustrates the optical in-line transmittance of the deposited samples. The deposited films under condition A showed relatively higher transmittance as compared to condition B and an absorption edge was observed for the film with V_2 = -0.6 V. Despite the film thickness obtained under condition B at V_2 = -0.4 V is slightly larger, yet the transmittance is still relatively high and an absorption edge was also observed. The appearance of the film is half transparent, while the other films have more black/opaque appearance.

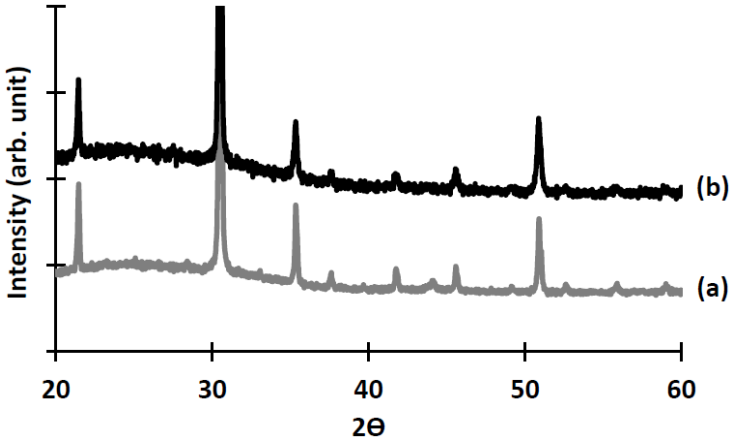

Fig. 6.5 XRD patterns of selected sample (a) ITO and (b) condition A with V_2 = -0.6 V.

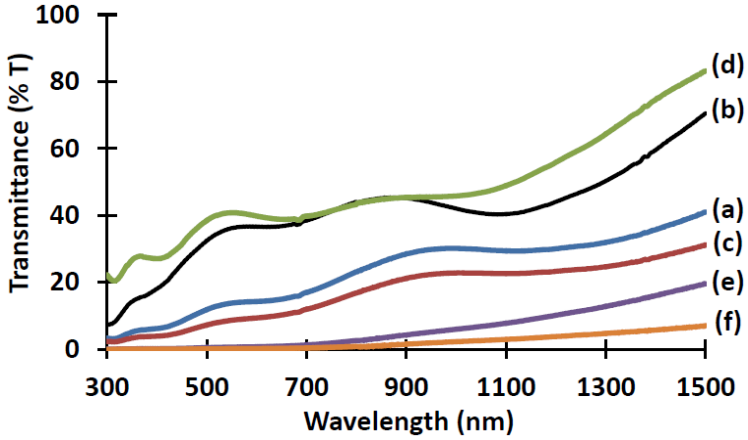

Fig. 6.6 Optical in-line transmittance of deposited samples: condition A, V_2: (a) -0.4 V, (b) -0.6 V, and (c) -0.8 V; condition B, V_2: (d) -0.4 V, (e) -0.6 V, and (f) -0.8 V.

To estimate the band gap for the films with an absorption edge, we plotted $(\alpha h\nu)^2$ and $(\alpha h\nu)^{1/2}$ vs. hν, where α is the absorption coefficient and hν is the photon energy. The plots are shown in Figs. 6.7(a)-6.7(c). The plot of $(\alpha h\nu)^{1/2}$ in Fig. 6.7(c) does not have a clear linear portion, while in the plot of $(\alpha h\nu)^2$ depicted in Figs. 6.7(a) and 6.7(b), extrapolations of the linear part would intersect the x-axis. The band gaps for the films under condition A with V_2 = -0.6 V and condition B with V_2 = -0.4 V were estimated around 2.3-2.45 eV.

Figure 6.8 depicts the photocurrent response in the PEC measurements for the selected deposited samples. The weak photoresponse was observed for all the samples

(including those not shown here) only in positive potential scans. The positive current increased as the sample was illuminated (on), and then decreased as the illumination was interrupted (dark-off). In the PEC measurement, the current due to the minority carrier (holes) was enhanced, thus, the results showed that the samples can be classified as n-type.

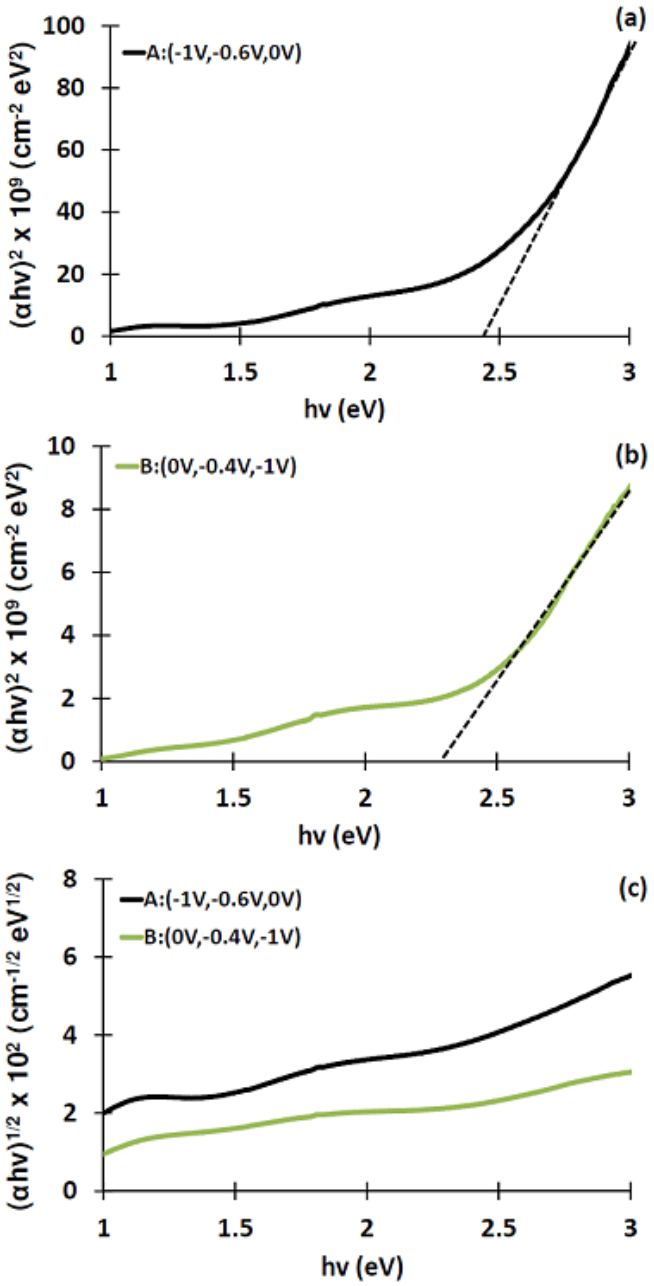

Fig. 6.7 Plots of $(\alpha h\nu)^2$ and $(\alpha h\nu)^{1/2}$ vs. hν for deposited samples: (a) condition A with V_2 = -0.6 V; (b) condition B with V_2 = -0.4 V; and (c) both the conditions.

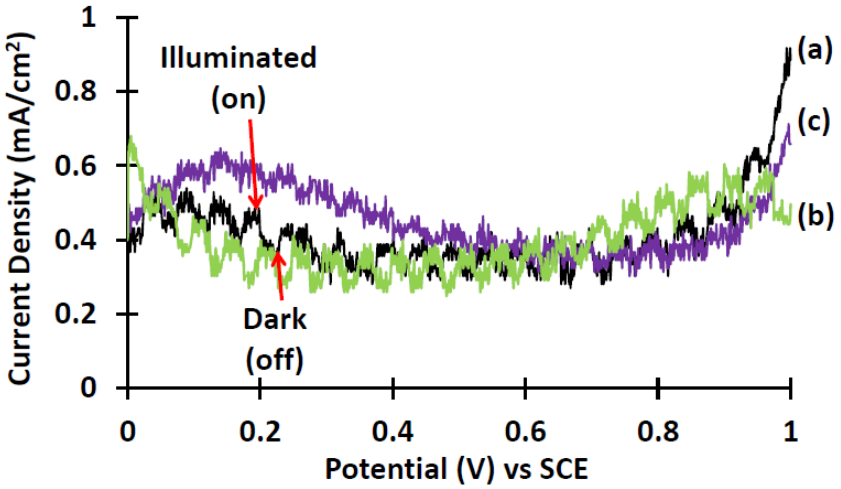

Fig. 6.8 Photocurrent responses in the PEC measurements for selected samples: (a) condition A with V_2 = -0.6 V; condition B with (b) V_2 = -0.4 V, and (c) -0.6 V.

In the visible wavelength range (400-700 nm), condition A (all V_2 values) and condition B (V_2 = -0.4 V) resulted in significant transmittance. The transmittance was relatively high (> 40%) for the samples under condition A with V_2 = -0.6 V and condition B with V_2 = -0.4 V. This is in contrast to our previous galvanostatic FeS_xO_y films for which within visible range, the transmittance was less than 2% [1]. The appearance of the films with galvanostatic mode was completely black/opaque meanwhile under three steps pulse using condition A (all V_2 values) and B (V_2 = -0.4 V), we found that the appearance turned into weakly transparent.

Based on the Raman results, our deposited films mainly composed of marcasite and $Fe_{1+x}S$ regardless of potential shifts direction and V_2 variation. Meanwhile in the compositional analysis by AES, all the films contain Fe, S, and O elements. The marcasite phase has the narrow band gap less than 0.30 eV [9-10], and thus is completely opaque for the visible range. The band gap of FeS (monophasic mackinawite phase) and Fe_2O_3 (α and β) was reported to be 1.87 eV [11] and 2.1-2.2 eV [12], respectively. Based on the plot of $(\alpha h\nu)^2$ vs. hν as depicted in Figs. 7(a) and 7(b), the band gap of those deposited films were between 2.3 and 2.45 eV, which is even larger than that of Fe_2O_3. So far there are no reports on the Fe-S-O films with such a large band gap. At present, we cannot explain why those films have such a large band

gap even though the narrow band gap marcasite is one of the dominant phases according to the Raman results. The amorphous nature, revealed by the XRD measurement, could be one of the possible reasons. However, the FeS_xO_y films deposited by galvanostatic or potentiostatic ECD are also amorphous but have black color and a small band gap [1,3-4]. Thus, the deposition pulse form (especially the V_2 value) seems to have strong impact on the film properties, but the mechanism is not understood.

Both the deposition conditions yield the films with weak n-type photoresponse (Fig. 8). Previously, we confirmed that the ITO substrate showed only very weak photosensitivity (photocurrent less than 1 $\mu A/cm^2$) in the PEC measurement [13]. Hence, the observed photocurrent mostly arises from the deposited films. The origin of the n-type conductivity is not clear but it is probably due to the oxygen content in the films. The O/Fe ratios in Figs. 3(a) and 3(b) for all the films were greater than 1 except for condition B with V_2 = -0.8 V, for which it is slightly lower than 1. Pure FeS_2 normally exhibits p-type conductivity, and Fe_2O_3 can exist in either n-type or p-type [14]. In a previous work of FeS_2 films fabricated by sulfurization of electrodeposited iron monosulfide films [15], they claimed that their n-type FeS_2 films were due to the diffusion of Ti atoms from the substrate which occurred during the sulfurization process. Our films have no other impurity such as In from the substrate and only contain Fe, S and O elements. Therefore, it can be considered that higher oxygen content in iron compound tends to enhance n-type character, compared with the pure sulfide.

Since our deposited films by three steps pulse ECD shows n-type conductivity and high transmittance in the visible range, it is possible to apply them as a window layer of solar cells. Solar cell fabrication can be paired either with a different p-type semiconductor material (heterojunction) such as Cu_2O or with a similar p-type material such as pyrite-FeS_2 (homojunction). In future studies, we will attempt to control the oxygen in FeS_xO_y films by annealing of the as-deposited samples in an air/N_2 environment and/or addition of complexing agents in the deposition solution, and investigate the effects of oxygen concentration on the photoresponse and band gap of the films.

6.4 Conclusion

FeS_xO_y thin films were deposited on ITO-coated glass substrates via three steps pulse ECD from an aqueous solution containing $Na_2S_2O_3$ and $FeSO_4$. All the films are amorphous with significant amount of oxygen content, contain mainly marcasite and mackinawite ($Fe_{1+x}S$), and show n-type conductivity. Large band gaps of 2.3-2.45 eV were obtained for the films deposited with the intermediate step potential V_2 of -0.6 V or -0.4 V. The change in photoresponse from p-type to n-type is most probably associated with the amount of oxygen content in the films.

References

[1] A. Supee and M. Ichimura, Jpn. J. Appl. Phys. 55 (2016) 081202.

[2] K. Yang, S. Kawai, and M. Ichimura, Thin Solid Films 573 (2014) 1-5.

[3] M. Ichimura, T. Kajima, S. Kawai, and K. Mibu, Jpn. J. Appl. Phys. 55 (2016) 038006.

[4] S. Kawai, R. Yamazaki, S. Sobue, E. Okuno, and M. Ichimura, APL Mater. 2 (2014) 032110.

[5] K. Omoto, N. Fathy, and M. Ichimura, Jpn. J. Appl. Phys. 45 (2006) 1500-1505.

[6] M. Umehara, Y. Takeda, H. Azuma, and T. Motohiro, Jpn. J. Appl. Phys. 51 (2012) 02BP10.

[7] R. Morrish, R. Silverstein, and C. A. Wolden, J. Am. Chem. Soc. 134 (2012) 17854-17857.

[8] J. A. Bourdoiseau, M. Jeannin, R. Sabot, C. Rémazeilles, and P. Refait, Corros. Sci. 50 (2008) 3247-3255.

[9] G. Willeke, R. Dasbach, B. Sailer, and E. Bucher, Thin Solid Films 213 (1992) 271-276.

[10] S. Nakamura and A. Yamamoto, Sol. Energy Mater. Sol. Cells 65 (2001) 79-85.

[11] M. Saeed Akhtar, A. Alenad, and M. Azad Malik, Mater. Sci. Semicond. Process. 32 (2015) 1-5.

[12] T. Hashimoto, T. Yamada, and T. Yoko, J. Appl. Phys. 80 (1996) 3184-3190.

[13] H. R. Dizaji and M. Ichimura, Mater. Sci. Eng.: B 158 (2009) 26-29.

[14] B. M. Warnes, F. F. Aplan, and G. Simkovich, Solid State Ionics 12 (1984) 271-276.

[15] A. Gomes, J. R. Ares, I. J. Ferrer, M. I. da Silva Pereira, and C. Sánchez, Mater. Res. Bull. 38 (2003) 1123-1133.

Chapter 7

Conclusion and recommendation

7.1 Conclusion of the research

This research mainly focuses on the electrochemical deposition (ECD) of SnS and FeS_xO_y thin films for solar cells applications. To alter the properties of the deposited single films, complexing agents are added in the deposition solution. Besides that, different ECD modes were also used for the deposition. For the heterostructures application, selected deposition conditions of single films were used with ZnO as the n-type partner. Based on the research done, several conclusions can be made as followed:

The effects of complexing agents for three steps pulse ECD of SnS thin films from a solution containing $Na_2S_2O_3$ and $SnSO_4$ were investigated. For the tartaric acid, the concentration used was up to 200 mM, while for the EDTA, it was limited to the 10 mM due to the solubility limit in the solution. The deposited films with complexing agents generally showed less oxygen content, larger sulfur content and tended to show clearer p-type photocurrent response as compared to without the agents. With low concentration of both complexing agents (1-10 mM), the film thickness was decreased and hence caused enhanced optical transmittance. In addition, both complexing agents resulted in retardation of Sn ions and a part of deposition (negative) current was consumed for reactions other than SnS deposition, such as H_2S generation. With high concentration (30-200 mM) of tartaric acid, the film thickness was slightly increased, yet the optical transmittance was still significantly high. Furthermore, the deposited films also show better crystallinity. In addition to the retardation effects on Sn ions, high concentration of tartaric acid also promoted the S reduction when its concentration is comparable to that of the sulfur source (100 mM $Na_2S_2O_3$). Obviously, the complexing agents are capable to alter the properties of the deposited SnS films, and overall, the properties of the film were improved with addition of EDTA and tartaric acid in the deposition solution.

ZnO/SnS heterostructures were fabricated for application to solar cells. ZnO film is easily dissolved in SnS solution, and thus, the structure of the heterostructure begins

with ITO substrate, followed by three steps pulse ECD of SnS (with/without 100 mM tartaric acid), then, two steps pulse ECD of ZnO on SnS, and lastly evaporated In on top of the film. The basic SnS solution contained $Na_2S_2O_3$ and $SnSO_4$, and for the ZnO, it contained $Zn(NO_3)_2$. The tartaric acid of 100 mM was selected as the complexing agent since it resulted in a large optical transmittance and no further reduction of oxygen content occurred for larger tartaric acid concentrations. The heterostructure consisted of poly-crystalline of SnS and ZnO layers, and larger size of ZnO grains was observed when 100 mM tartaric acid was used for the SnS deposition. The fabricated heterostructures showed clear rectifying properties with some leakage current. Under AM1.5, both the heterostructures showed very weak photovoltaic properties: the open circuit voltage less than 0.01 V and the short circuit current density less than 1 $\mu A/cm^2$. Although the SnS film properties were improved as mentioned above with 100 mM tartaric acid addition, the solar cell performance was not improved. Thus, the leakage current and very weak photovoltaic properties are thought to be due to poor ZnO/SnS interface properties.

The effects of complexing agents in galvanostatic ECD of FeS_xO_y thin films with a solution containing $Na_2S_2O_3$ and $FeSO_4$ were studied. The concentrations of complexing agents, i.e., tartaric acid and lactic acid were up to 50 mM and 167 mM, respectively. All the deposited films were amorphous with weak p-type photocurrent response. Comparing to deposition without the agents, the complexing agents generally caused oxygen content reduction, increase in the thickness, and relatively small grain size with improved uniformity. A significant reduction in oxygen content was obtained at high concentrations of tartaric acid (> 10 mM) and lactic acid (56-167 mM). Therefore, both the acids as the complexing agents resulted in retardation of oxide formation via the mechanism of $Fe(OH)_2$ suppression. However, the optical and electrical properties were not improved by the reduction in oxygen content. Clearly, the oxygen atoms seem to have no significant effects on the properties of amorphous iron sulfide films, and this is probably because the local bonding configuration around Fe atoms is not altered by the substitution of sulfur with oxygen.

ZnO/FeS_xO_y heterostructures were fabricated for application to solar cells. The structure of the heterostructure was arranged in the following sequence: ITO substrate,

galvanostatic ECD of FeS_xO_y (with/without complexing agents), two steps pulse ECD of ZnO on FeS_xO_y, and evaporated In on top of the film. The basic FeS_xO_y solution contained $Na_2S_2O_3$ and $FeSO_4$ and for the ZnO, it contains $Zn(NO_3)_2$. Tartaric acid (30 mM) and lactic acid (56 mM) were used as the complexing agents in the FeS_xO_y deposition because the oxygen content drastically reduced at these amounts of concentrations and because further increases in the concentration of complexing agents only resulted in small reduction in oxygen content. All the heterostructures consisted of amorphous FeS_xO_y and poly-crystalline ZnO layers and exhibited rectifying properties with significant large of leakage current. This indicates that the oxygen content in the FeS_xO_y film has no influences toward the performance of the solar cells. Furthermore, the heterostructures perhaps have poor interface properties associated with trap states.

The three steps pulse ECD was adopted for the first time in FeS_xO_y deposition from an aqueous solution containing $Na_2S_2O_3$ and $FeSO_4$ and the deposited films were characterized. ECD was performed using periodic three steps pulse with intermediate V_2 manipulation under two different condition namely condition A (potential shifts from negative to positive) and condition B (potential shifts from positive to negative). All the deposited films were amorphous. In Raman measurements, peaks attributed to marcasite and $Fe_{1+x}S$ were observed. The O/Fe ratio is larger than unity. The films under condition A with V_2 = -0.6 V and condition B with V_2 = -0.4 V showed a band gap which was estimated around 2.3-2.45 eV, larger than literature value of Fe_2O_3 (2.1 eV). In the photoelectrochemical measurement, n-type behaviour was confirmed.

Overall, with the additions of complexing agents in the deposition solution, the properties of SnS and FeS_xO_y thin films were altered. The agents were capable to retard metal (Sn, Fe) reductions via metal-complex formation, promote S reduction, and suppress hydroxide formation. Although the properties of SnS and FeS_xO_y films deposited with the complexing agents were improved as mentioned above, their photovoltaic properties in the fabricated heterostructures did not seem to be affected. On the other hand, in the three steps pulse FeS_xO_y, the pulse form especially the intermediate step (V_2) significantly affected the optical and electrical properties of the deposited films.

7.2 Recommendation for the future work

Based on the results and the conclusions obtained from this research, some suggestions for future work in the same area are recommended as followed:

In this research, complexing agents were used in ECD of SnS and FeS_xO_y thin films. Different concentrations of complexing agents namely EDTA, tartaric acid and lactic acid were added in the electrolyte solution of both thin films and the complexing agents were mainly results in retardation of the metal ions deposition, suppressed metal hydroxide formation (reduced oxygen content), and promotes sulfur reduction. Other than mentioned, there are a lot of complexing agents available in the market. Each complexing agent probably results in different effects. Thus, it is great opportunities to extend the ECD of both films using different complexing agents such as triethanolamine (TEA), sulfosalicylic acid, glycine, citric acid, and etc. and investigate the effects of those complexing agents on the properties of the deposited films. Pre-evaluation of the complexing agents can be done through visual observation of chemical stability of the basic electrolyte solution with complexing agents and initial information related to deposition can be obtained via cyclic voltammetry.

In the solar cells applications, for instance, for the fabrication of ZnO/SnS heterostructure, the SnS absorber layer was firstly deposited on the ITO substrate instead of ZnO window layer. Normally, the light is incident on the window layer side in the current density-voltage (J-V) measurement. However, due to dissolution of the ZnO film in the SnS deposition solution, the heterostructure was irradiated on the ITO glass (SnS) side. This kind of window-absorber layer sequence partly results in small output during the J-V measurement of the heterostructure under AM 1.5 condition. This is because majority of the photo-generated carriers could be absorbed by the SnS absorber layer before reaching the p-n junction (ZnO/SnS interface). Thus, another non-toxic and cheaper material which is more stable in the SnS deposition solution should be considered as a window layer. This materials supposed to have an appropriate band gap value and also well-matched lattice parameters and crystal structures to SnS so that the recombination rate at the heterointerface could be minimized and as a consequences, an efficient heterostructure solar cells could be obtained.

The interface properties between absorber and window layers as well as the properties of each layer are very important in determining the performance of the heterostructures solar cells. It will be useful to determine the effects of mutual inter-diffusion at the interface on heterostructures performance by depth profiling using Auger electron spectroscopy. Furthermore, insertion of a very thin layer at the interface will probably be able to reduce the formation of undesired secondary/impurities phases and result in a clearly defined interface. By having a clear interface, the current leakages caused by inter-diffusion of grain from each layers could be minimized and thus the performance of the heterostructures could be improved.

The electrolyte solution stability is one of the important factors considered prior to the deposition. The sequences of the chemical addition normally affect the pH changes. Therefore precaution in term of the chemical sequences should be done first for the new chemical additions so that the uncontrolled parameters such as unwanted chemical reactions and precipitation could be eliminated and the deposited film with desired properties could be obtained.

The three steps pulse ECD was implemented in FeS_xO_y deposition and the effects of potential shifts direction with the intermediate potential V_2 variation on the deposited films were studied. All the films showed n-type photoresponse and mostly contains O/Fe > 1. The deposition pulse form (especially the V_2 value) results in significance impact on the optical properties. Therefore, it is suggested to further investigate the effects of oxygen content for both the conditions on the optical (transmittance and band gap) and the electrical (photocurrent response) properties of the FeS_xO_y films. The oxygen content could be varied either by means of annealing the deposited samples in air/N_2 environment and/or by introducing the complexing agents in the deposition solution. Then, a solar cell based on FeS_xO_y films for as-deposited/annealed/with complexing agents can be fabricated either paired with different p-type semiconductor material (heterojunction) such as Cu_2O or with similar p-type material such as pyrite-FeS_2 (homojunction).

Journal

[1] **A. Supee**, Y. Tanaka, and M. Ichimura

"Effects of complexing agents on three steps pulse electrodeposited SnS thin films"

Mater. Sci. Semicond. Process. 38 (2015) 290-297.

[2] **A. Supee** and M. Ichimura

"Effects of tartaric acid on electrochemical deposition of SnS in ZnO/SnS heterostructures"

Trans. Mat. Res. Soc. Jpn. 41 (2016) 193-195.

[3] **A. Supee** and M. Ichimura

"Effects of complexing agents on electrochemical deposition of FeS_xO_y thin films"

Jpn. J. Appl. Phys. 55 (2016) 081202.

[4] **A. Supee** and M. Ichimura

"Three steps pulse electrochemical deposition of FeS_xO_y thin films and their characterization"

Submitted to Mater. Res. Exp..

Presentation

[1] **A. Supee** and M. Ichimura

"Effects of tartaric acid on electrochemical deposition of SnS in ZnO/SnS heterostructures"

25th Annual Meeting of Materials Research Society of Japan (MRS-J) 08-10 December 2015,

Presented: 08 December 2015-Yokohama Media & Communications Center (Hall), Yokohama, Japan.

[2] **A. Supee** and M. Ichimura

"Effects of tartaric acid on electrochemical deposition of FeS_xO_y films"

International Seminar on Nanoscience and Nanotechnology 2016 (NANO-SciTech 2016) 27-28 February 2016,

Presented: 27 February 2016-Institute of Leadership, Assessment and Development (ILEAD), UiTM Shah Alam, Malaysia.